JACS Au
AN OPEN ACCESS JOURNAL OF THE AMERICAN CHEMICAL SOCIETY

pubs.acs.org/jacsau
Perspective

Excited Organic Radicals in Photoredox Catalysis

Björn Pfund* and Oliver S. Wenger*

Cite This: JACS Au 2025, 5, 426−447
Read Online
ACCESS | Metrics & More | Article Recommendations | Supporting Information

ABSTRACT: Many important synthetic-oriented works have proposed excited organic radicals as photoactive species, yet mechanistic studies raised doubts about whether they can truly function as photocatalysts. This skepticism originates from the formation of (photo)redox-active degradation products and the picosecond decay of electronically excited radicals, which is considered too short for diffusion-based photoinduced electron transfer reactions. From this perspective, we analyze important synthetic transformations where organic radicals have been proposed as photocatalysts, comparing their theoretical maximum excited state potentials with the potentials required for the observed photocatalytic reactivity. We summarize mechanistic studies of structurally similar photocatalysts indicating different reaction pathways for some catalytic systems, addressing cases where the proposed radical photocatalysts exceed their theoretical maximum reactivity. Additionally, we perform a kinetic analysis to explain the photoinduced electron transfer observed in excited radicals on subpicosecond time scales. We further rationalize the potential anti-Kasha reactivity from higher excited states with femtosecond lifetimes, highlighting how future photocatalysis advancements could unlock new photochemical pathways.

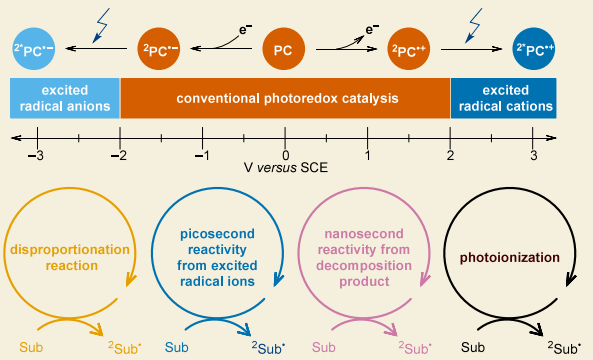

KEYWORDS: *Photocatalysis, Mechanistic Analysis, Electron Transfer, anti-Kasha Reactivity, Picosecond Photochemistry*

1. INTRODUCTION

Electronically excited organic radicals have been identified as potentially extremely potent photocatalysts, reaching electrochemical potentials greater than +3 and −3 V versus SCE.[1,2] Numerous synthetically motivated studies invoked excited radicals as the photoactive species,[1−28] but mechanistically oriented studies questioned whether excited organic radicals can act as true photocatalysts. The two main reasons for this skepticism are the observed formation of (photo)redox-active degradation products,[29−31] and the picosecond decays of the excited radicals, a time frame too short for diffusion-based single electron transfer (SET).[32−35] One way to enable picosecond SET would be preassociation between the organic radicals and the substrate,[36,37] but until recently, the experimental evidence for this hypothesis has been scant.[38] While the synthetic value of using excited organic radicals for thermodynamically challenging reactions is undisputed,[36,37,39] the mechanistic aspects remain debatable. This Perspective aims to identify the fundamental preconditions for excited organic radicals to act as true photocatalysts, thus advancing the rational design of photoredox reactions. We begin with a brief recapitulation of the different methods to form organic radicals and then move on to a collective analysis of reactions that claim organic radical photoreactivity. This analysis leads us to clear insights that define the application potential and limits of excited organic radicals in modern photoredox catalysis. The upshot is that there could be overlooked aspects, such as anti-Kasha reactivity, which, if made broadly accessible in a rationally predictable manner, could significantly influence the field of photochemistry.

2. METHODS FOR THE GENERATION OF EXCITED RADICALS

2.1. Consecutive Photoinduced Electron Transfer (ConPET)

One of the first, if not the first study to claim excited radicals as photocatalysts on a broad preparative scale used a consecutive photoinduced electron transfer (ConPET) excitation strategy (Figure 1a),[22] similar to a $[Cu(dmp)_2]^+$ (dmp = 2,9-dimethyl-1,10-phenanthroline) system, where ConPET was initially described but not used in photoredox catalysis.[40] In this two-photonic ConPET mechanism, the organic precursor compound ([PC]) absorbs the first photon, forming its excited state (*[PC], Figure 1a). Subsequent SET, either from a sacrificial electron donor (e.g., Et_3N)[22,41] or to an electron acceptor (e.g., SF_6),[42] can result in the generation of the organic radical (^{2}[PC]$^\bullet$, Figure 1a). Eventually, this radical is excited to activate

Received: October 16, 2024
Revised: December 21, 2024
Accepted: December 27, 2024
Published: January 29, 2025

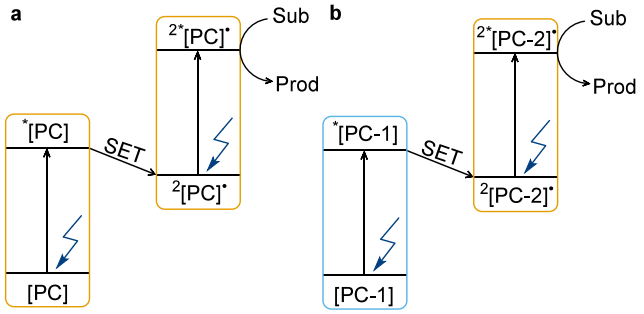

Figure 1. a. Consecutive photoinduced electron transfer (ConPET) strategy to generate excited radicals (^{2*}[PC]$^{\bullet}$) to initiate challenging substrate activations.[22] **b.** Consecutive photoinduced electron transfer using two different light absorbers ([PC-1] and ^{2}[PC-2]$^{\bullet}$).[38,43,47]

otherwise redox-inert substrates. The ConPET mechanism is often compared to the Z-scheme of natural photosynthesis,[43−45] but an important difference is that nature uses two distinct and mutually independent light absorbers. The interdependence of [PC] and ^{2}[PC]$^{\bullet}$ in the ConPET excitation strategy restricts the search for suitable systems and limits the maximally achievable redox power.[43] This is because system design typically requires that both the precursor compound and the resulting radical absorb visible light. However, by using a photosensitizer ([PC-1], Figure 1b) to generate the redox-active organic radical (^{2}[PC-2]$^{\bullet}$) through SET or energy transfer (EnT) separates the two light-absorbing events, allowing for greater redox power,[38] or the use of lower-energy input light.[43,46]

2.2. Electrochemically Mediated Photoredox Catalysis (e-PRC)

Photoactive organic radicals can also be generated electrochemically using a low-magnitude potential as highlighted in several review articles.[36,39,48] The absorbed photon energy then adds to the applied potential upon photoexcitation. Compared to the ConPET mechanism, the e-PRC methodology, sometimes also called electron-primed photoredox catalysis, has the advantage that the precursor compound PC no longer needs to absorb visible light. Further, no sacrificial redox reagents are required. However, a somewhat more sophisticated experimental setup is needed, and overpotential can lead to decomposition or side reactions.

2.3. Chemically Primed Photoinduced Electron Transfer

Organic radicals are also accessible chemically instead of electrochemically, which has been mostly used in mechanistically oriented studies.[23,24] Employing strong redox reagents for radical formation may cause side reactions, limiting its practicability in synthetic contexts. Specific examples explored until now include 9,10-dicyanoanthracene (DCA) and naphthalene monoimide (NMI), which were reduced to their monoanionic forms using KC_8.[24]

3. EXCITED STATE REACTIVITY OF ORGANIC RADICALS

For leveraging organic radicals as photocatalysts, assessing their theoretical maximal excited state redox potential is essential to guide the selection of suitable reactants. The lowest doublet excited state redox potential of the proposed radical ions can be estimated using the well-known Rehm−Weller equation for radical anions: $E(\mathrm{PC}/^{2*}\mathrm{PC}^{\bullet-}) \approx E(\mathrm{PC}/^{2}\mathrm{PC}^{\bullet-}) - E_{\mathrm{D1}} \times e$, and for radical cations: $E(^{2*}\mathrm{PC}^{\bullet+}/\mathrm{PC}) \approx E(^{2}\mathrm{PC}^{\bullet+}/\mathrm{PC}) + E_{\mathrm{D1}} \times e$. Here, e is the elementary charge, $E(\mathrm{PC}/^{2}\mathrm{PC}^{\bullet-})$ or $E(^{2}\mathrm{PC}^{\bullet+}/\mathrm{PC})$ represents the ground state redox potential of the precatalyst, and E_{D1} is the transition energy of the organic radical (in eV), with D_1 denoting the lowest-energy doublet excited state.[49] (The lowest excited state is a doublet due to the presence of one unpaired electron). Accessing the ground state redox potential ($E(^{2}\mathrm{PC}^{\bullet+}/\mathrm{PC})$ or $E(\mathrm{PC}/^{2}\mathrm{PC}^{\bullet-})$) via cyclic voltammetry is a standard method.[50] The D_1 excited-state energy of the organic radical (E_{D1}) is usually obtained from UV−vis absorption spectra of the radicals, as luminescence is commonly not observed due to the picosecond excited states lifetimes. Higher-lying excited states (D_n, $n > 1$) typically undergo internal conversion (IC) to D_1 on a subpicosecond time scale.[35,51] Consequently, it is assumed that reactivity can only occur from the lowest excited state, with excited state lifetimes in the picosecond range. Therefore, the most red-shifted UV−vis absorption band, corresponding to the lowest excited state, should normally be used to estimate the transition energy of organic radicals.

In this Chapter, we compare the theoretically calculated excited state redox potentials with the observed reactivity, which provides indirect evidence of whether the excited radicals can serve as a catalytically active species.[43] Examples where reactivity surpasses the theoretically predicted excited state potentials suggest the involvement of alternative mechanisms.[14,19,20,27,28,52−58] Many of the considered substrates undergo irreversible redox processes, making it challenging to accurately determine their true thermodynamic redox potentials. Nonetheless, cyclic voltammetry can provide reasonable estimates of their redox potentials.

3.1. Reductive Catalysis Using Excited Organic Radicals

Excited radicals have found broad applications in challenging reductive activation of C(sp^2)- and C(sp^3)-halide bonds (Figure 2b-n). The literature-known organic radical photocatalysts are summarized and ranked along increasing reduction power, determined from the theoretical excited state reduction potentials described above. In cases where the reactivity of organic radical photocatalysts exceeds the theoretical limit, the gray and blue hatched areas in Figure 2a mark the range of achieved reduction potentials.

The ConPET excitation strategy was introduced in a synthetically oriented context for activating electron-deficient aryl halides (I, Br, Cl), employing PDI$^{\bullet-}$ as a presumed photocatalyst.[22] Following SET from the excited PDI$^{\bullet-}$ to the aryl-halide, the resulting aryl radical can be captured by a hydrogen atom donor, forming an H—C(sp^2) bond, or by trapping agents like *N*-methyl pyrrole derivatives, forming C(sp^2)—C(sp^2) bonds (Figure 2g).[22,59,60] In a similar study, PDI-based hybrid materials ($(PDI)_2{\cdot}SiW_{12}O_{40}$) served as ConPET photocatalysts for the reductive activation of perfluoroalkyl iodide, leading to perfluoroalkylation in the presence of an alkene (Figure 2f).[61] PDI is widely used in ConPET,[22,59−62] and it is noteworthy that the most challenging substrate that was successfully activated requires a significantly more negative redox potential of approximately −2.1 V versus SCE (estimated from 2-chlorobenzonitrile)[63] than the theoretical excited state reduction potential of ^{2*}PDI$^{\bullet-}$ (−1.7 V versus SCE).[22]

Similar to PDI$^{\bullet-}$, the reductive activation of electron-deficient aryl-halides (Figure 2) has also been achieved using 9-hydroxyl-1-oxophenalenylene (Phen),[64] 1,8-dihydroxyanthraquinone (Aq−OH),[16] naphthalene diimide (NDI),[65,66] or donor−acceptor compounds (D-A PC)[67] as ConPET photocatalysts.

https://doi.org/10.1021/jacsau.4c00974
JACS Au 2025, 5, 426−447

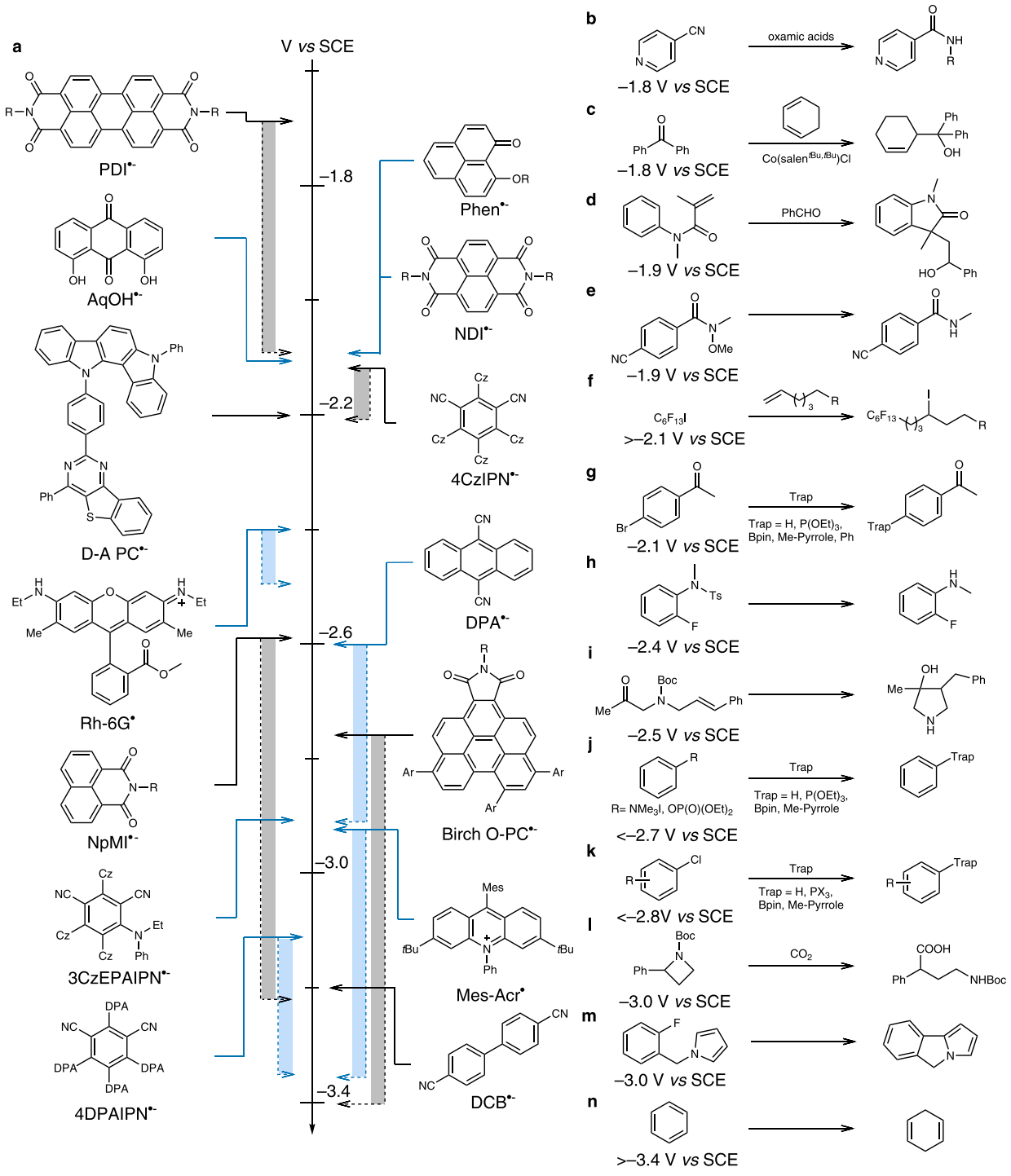

Figure 2. a. Excited-state redox potentials of various organic radicals determined using the Rehm−Weller equation (arrows). The molecular structures shown are those of the closed-shell precursors prior to radical formation. In cases where the observed reactivity surpasses the theoretical reduction potential, the blue and gray hatched regions represent the deviation to the reduction potentials of activatable substrates. **b**−**m.** Previously performed reactions claimed to utilize the reactivity of excited radicals and their required reduction potentials: **b.** Radical−radical cross-coupling of 4-cyanopyridine and oxamaic acid.[53] **c.** Reductive coupling of dienes with ketones.[54] **d.** Ketyl radical coupling reactions with acrylamide.[52] **e.** N−O bond cleavage reaction of Weinreb amides.[14] **f.** Perfluoroalkylation reaction.[61] **g.** Debromination reaction of aryl bromides.[10,15,16,22,24,27,43,59,60,64−71] **h.** Detosylation reactions.[2,55] **i.** Ketone olefin coupling reaction.[12] **j.** Aryl C(sp^2)−N and C(sp^2)−O bond cleavage reaction.[20,57] **k.** Dechlorination reaction of unactivated aryl chlorides.[2,19,20,24,27,28] **l.** Carboxylation reaction of C−N bonds in cyclic amines with CO_2.[58] **m.** Base-promoted homolytic aromatic substitution (BHAS) of an aryl fluoride.[38] **n.** Birch reduction of benzene derivatives.[13]

The resulting aryl radical intermediates can be captured by various trapping agents, including triethyl phosphite (P-$(OEt)_3$),[64] benzene,[65,66] bis(pinacolato)diboron (B_2pin_2),[67] or *N*-methyl pyrrole derivatives (Figure 2 and Table 1, entries 2−5).[16] In contrast to PDI, these ConPET photocatalysts exhibit good agreement between observed and theoretically calculated excited-state redox potentials of approximately −2.2 V versus SCE.

https://doi.org/10.1021/jacsau.4c00974
JACS Au 2025, 5, 426−447

Table 1. Summary of Selected Key Properties of Known Reactive Excited Organic Radicals and the Corresponding Precursor Compound

	$PC^{\bullet-}$	E (PC/$PC^{\bullet-}$)/V vs SCE	E_{D1}/eV[a]	τ_{D1}/ps	E (^{2}*$PC^{\bullet-}$/PC)/V vs SCE calc.[b]	E (^{2}*$PC^{\bullet-}$/PC)/V vs SCE obs.[c]	applications
1	$PDI^{\bullet-}$	−0.4[22]	1.3[22]	160[35]	−1.7	−2.1[d]	Reductive activation of electron-deficient bromo- and chloroarenes.[22,59,60] Perfluoroalkylation reaction.[61,62]
2	$Phen^{\bullet-}$	−0.7[64]	n/a (D_1)[e]	n/a	n/a (D_1)	−2.1[f]	Reductive activation of iodoarenes, as well as electron-deficient bromo- and chloroarenes.[64]
			2.5 (D_n)[64]		−3.2 (D_n)		
3	$Aq{-}OH^{\bullet-}$	−0.6[16]	1.5[16]	n/a	−2.1	−2.1[d]	Reductive activation of electron-deficient bromo- and chloroarenes.[16]
4	$NDI^{\bullet-}$	−0.5[64]	1.6[64]	14[51]	−2.1	−1.9[g]	Reductive activation of electron-deficient bromoarenes.[65,66]
5	D-A $PC^{\bullet-}$	−1.5[67]	0.7[67]	64[67]	−2.2	−1.7[h]	Reductive activation of electron-deficient bromoarenes[67]
6	$4CzIPN^{\bullet-}$	−1.24	0.8	27[72]	−2.0 (D_1)[i]	−2.2[k]	Reductive N−O bond cleavage of Weinreb amides.[14] Radical−radical cross-coupling of 4-cyanopyridine and oxamic acid.[53] Reductive ketyl radical coupling reaction with *N*-aryl acrylamides.[52] Dual-catalyzed reductive coupling of dienes and ketones.[54] Dual-catalyzed CO_2 reduction.[55] Direct C(sp^3)−H arylation of unprotected benzyl anilines and alkylarenes.[73] Formation of carbon radicals from sulfoxonium ylides in aqueous solution.[74]
			2.4		−3.6 (D_n)[j]	−2.9[n]	
7	$Rh\text{-}6G^{\bullet}$	−0.9[15]	1.5[75]	0.35[75]	−2.4	−2.5[l]	Reductive activation of electron-rich bromoarenes,[15,68,69] and electron-deficient chloro(hetero)arenes.[70]
8	$DCA^{\bullet-}$	−0.9[10]	1.7[42]	3[33]	−2.6	−2.6[m] (ConPET)	Reductive activation of bromo- and chloro(hetero)arenes.[10,24,27,43,71] Reductive detosylation reactions of phenolic and nitrogen-containing substrates.[43]
						−2.9[n] (e-PRC)	
9	$NMI^{\bullet-}$	−1.3[29]	1.4[29]	24[29]	−2.7	−3.4[o]	Reductive activation of electron-rich chloroarenes.[24,28] Reductive deoxygenation reaction of C(sp^3)-O bonds using phosphinated alcohols.[21]
10	Birch O-$PC^{\bullet-}$	−1.2[13]	1.6[13]	10[76]	−2.8	−3.4[p]	Birch reduction.[13]
11	$Mes\text{-}Acr^{\bullet}$	−0.6[2]	2.3 (D_1)[q]	100[2]	−2.9 (D_1)[q]	−2.9[l]	Reductive activation of electron-rich chloroarenes and detosylation reactions of phenolic and nitrogen-containing substrates.[2] Reductive activation of electron-rich carbonyls for ketone-olefin coupling reactions.[12]
			2.8[r] (TICT)		−3.4[r] (TICT)		
12	3CzEPA-$IPN^{\bullet-}$	−1.40[19]	n/a	n/a	n/a	−2.9[l]	Reductive activation of electron-rich chloroarenes.[19]
13	$4DPAIPN^{\bullet-}$	−1.5	1.6[s]	21[72]	−3.1	−3.4[o]	Reductive C(sp^2)−N and C(sp^2)−O bond cleavage reactions.[20,57] Reductive activation of 2-aryl-aziridines and 2-carbonyl-azetidines.[58] Reductive activation of electron-rich chloroarenes.[20]
14	$DCB^{\bullet-}$	−1.6[38,77]	1.6[38]	3[38]	−3.2	−3.0[t]	Base-promoted homolytic aromatic substitution (BHAS) reaction of aryl halides and intramolecular radical nucleophilic substitution reaction of 2-halide-*N*-phenylanilines to carbazole.

[a]The lowest doublet excited state energies (E_{D1}) were estimated by taking the point on the low-energy side of the absorption spectra of the photocatalysts, at which 10% of the maximum absorption is reached. [b]The excited state redox potentials (E (^{2}*$PC^{\bullet-}$/PC)) were calculated using the Rehm−Weller equation E (^{2}*$PC^{\bullet-}$/PC) ≈ E (PC/$PC^{\bullet-}$) − $E_{D1} \times e$, with the elementary charge e, the ground state potentials (E (PC/$PC^{\bullet-}$), column 3), and the D_1 energy (E_{D1}, column 4). [c]Determined by analyzing the substrate with the lowest reduction potentials. [d]Estimated from 2-chlorobenzonitrile.[63] [e]Absorption spectrum of radical anion only reported up to 520 nm. Hence, lower energy absorption bands of the radical anion, as classically observed for organic radicals, cannot be excluded. [f]Estimated from 2-iodonaphthalene.[64] [g]Estimated from 4-bromobenzonitrile.[66] [h]Estimated from 4-bromoacetophenone.[78] [i]Estimated using DFT calculation. [j]Estimated from the lowest UV−vis absorption band. [k]Estimated from 1,4-dichlorobenzene.[55] [l]Estimated from *p*-trifluoromethylphenyl bromide.[43] [m]Highest achieved redox potential using a ConPET mechanism,[10,24,27,43,71] estimated from 2-acetyl-4-chlorothiophene.[71] [n]Highest achieved redox potential using an e-PRC mechanism,[27] estimated from 4-chloroanisol.[2] [o]Estimated from 1,3-di-*tert*-butyl-5-chloro-2-methoxybenzene.[28] [p]Estimated from benzene.[13] [q]Estimated based on a claimed emission of the $Mes\text{-}Acr^{\bullet}$ despite a more red-shifted absorption band.[2] [r]Claimed reactivity from a higher excited, twisted intramolecular charge-transfer (TICT) state.[2] [s]DFT calculation suggests an additional transition at ∼1500 nm.[79] [t]Estimated from fluorobenzene.[80]

https://doi.org/10.1021/jacsau.4c00974
JACS Au 2025, 5, 426−447

2,4,5,6-Tetra(9H-carbazol-9-yl)isophthalonitrile radical anion (4CzIPN$^{\bullet-}$) is a widely employed photocatalyst in challenging reductions (Table 1, entry 6), such as N—O bond cleavage of Weinreb amides, which typically rely on relatively harsh conditions (Figure 2e).[14] Moreover, 4CzIPN$^{\bullet-}$ enables redox-neutral ketyl radical coupling reactions of carbonyls with *N*-aryl acrylamides,[52] as well as radical−radical cross-coupling reactions, activating 4-cyanopyridine to form *N*-substituted nicotinamides in the presence of oxamic acid derivatives (Figure 2b).[53] Notably, 4CzIPN$^{\bullet-}$ also finds application in dual catalysis systems.[54,55] One example enables the intermolecular reductive coupling of dienes and styrene with ketones using 4CzIPN$^{\bullet-}$ in combination with Co(salen^{tBu,tBu})Cl.

Employing the ConPET mechanism facilitates the formation of the catalytically active cobalt hydride and SET to ketones, resulting in ketyl radical formation (Figure 2c).[54] Another dual catalytic system utilizes 4CzIPN$^{\bullet-}$ for single-electron transfer to a bis(terpyridine)ruthenium(II) cocatalyst, enabling CO_2 reduction to CO in solution.[55] With the theoretically obtained D_1 energy of 0.8 eV, using DFT calculations,[72] an excited state reduction potential of −2.0 V versus SCE can be estimated. This matches the most difficult to reduce substrate used in a ConPET excitation strategy, especially considering the uncertainty of the estimated D_1 energy using DFT calculations.[55]

Rhodamine 6G radical (Rh-6G$^{\bullet}$) has demonstrated the reductive activation of electron-rich (hetero)aryl-bromides[15,68] and electron-deficient (hetero)aryl-chlorides,[70] forming the corresponding (hetero)aryl radicals (Table 1, entry 7). Various trapping reagents such as *N*-methyl pyrrole derivatives,[15,70] pyrrole derivatives,[15,70] benzene,[15,70] 1,2-diphenylethylene,[15,70] or triethyl phosphite,[68] could be employed to form different C(sp^2)—C(sp^2) and C(sp^2)—P(sp^3) bonds by trapping the (hetero)aryl radical intermediates (Figure 2g). The theoretical limit of the excited state redox potential of −2.4 V versus SCE is in good agreement with the most challenging tested substrates (i.e., *p*-trifluoromethylphenyl bromide with a reduction potential of −2.5 V versus SCE).[43]

9,10-Dicyanoanthracene radical anion (DCA$^{\bullet-}$) shows similar reactivity to Rh-6G$^{\bullet}$ (Table 1, entry 8). Employing a ConPET excitation strategy, both electron-rich bromo-(hetero) arenes and electron-deficient chloro-(hetero) arenes were activated under blue light irradiation (Figure 2g).[10,71] Comparable reactivity was observed when employing a ConPET excitation strategy with a second chromophore. In this system, DCA$^{\bullet-}$ is formed through red light-induced electron transfer from $[Cu(dap)_2]^+$ (dap = 2,9-dianisyl-1,10-phenanthroline) to DCA. Upon absorption of a second red photon by DCA$^{\bullet-}$, the redox-active ^{2}*DCA$^{\bullet-}$ is formed, facilitating dehalogenation of aryl-bromides or aryl-chlorides (Figure 2g), as well as detosylation reactions (Figure 2h).[43] Notably, no substrate could be activated with a significantly more negative reduction potential than the theoretical maximum of −2.6 V versus SCE.[10,43,71] However, employing an e-PRC[27] method or chemical formation of DCA$^{\bullet-}$,[24] the activation of electron-rich aryl-chlorides in moderate to good yields (21−90%) was achieved.[70] These substrates often exhibit reduction potentials as low as −2.9 V versus SCE (Figure 2j), which would surpass the expected reduction potential of ^{2}*DCA$^{\bullet-}$. Similar behavior was reported for naphthalene monoimide radical anions (NMI$^{\bullet-}$).[28] When employing e-PRC or chemical formation of radical anions, electron-rich aryl-chlorides were activated with reduction potentials as negative as −3.4 V versus SCE (Figure 2k). This is obviously significantly more negative than the −2.7 V versus SCE that ^{2}*NMI$^{\bullet-}$ is estimated to provide (Table 1, entry 9).

A modified ConPET excitation strategy employed benzo-[ghi]perylene monoimides (Birch-O-PC) as a precatalyst (Table 1, entry 10).[13] The photoactive Birch-O-PC$^{\bullet-}$ compound is generated by adding hydroxide (OH^-) to the imide, forming the covalent hydroxide adduct ([Birch-O-PC−OH]$^-$). Following photoexcitation of [Birch-O-PC−OH]$^-$, an intramolecular SET is proposed from OH^- to the imide, forming the radical anion Birch-O-PC$^{\bullet-}$ and OH$^{\bullet}$. This step was invoked as commonly used electron donors cannot reduce the excited Birch-O-PC. Upon photoexcitation, the resulting ^{2}*Birch-O-PC$^{\bullet-}$ effectively reduced various benzene derivatives to 1,4-cyclohexadiene products in yields ranging from 24% to 91% (Figure 2n). These reductions require exceptionally powerful reduction potentials of −3.4 V versus SCE, marking a significant breakthrough in synthetic photoredox catalysis. However, the estimated excited state redox potential appears insufficient with −2.8 V versus SCE. This discrepancy was explained in a later study, which included the same research group,[76] in which the underlying mechanism and the true photoactive catalyst were identified (see discussion below).

Similarly strong reduction potentials were claimed using a modified acridinium salt (Mes-Acr$^+$) as a precatalyst (Table 1, entry 11).[2] Employing a presumed ConPET excitation strategy, remarkable reactivities were observed, such as hydro-dehalogenation reactions of various electron-poor and electron-rich aryl-bromides and chlorides (Figure 2k), as well as detosylation reactions (Figure 2h), which typically require reduction potentials as low as −2.9 V versus SCE.[2] Additionally, Mes-Acr$^{\bullet}$ could be used as a photocatalyst to activate electron-rich carbonyls for ketone-olefin coupling (Figure 2i), further demonstrating the usability of the catalytic system.[12] In these studies, the theoretically achievable excited state reduction potential was estimated based on a claimed twisted intramolecular charge transfer (TICT) state with a transition energy of 2.5 eV. This TICT state would result in an extremely negative excited state redox potential of −3.4 V versus SCE. However, considering the lowest claimed excited state transition energy of 2.3 eV, a still highly reactive excited state reduction potential of −3.2 V versus SCE is instead achieved. It is worth noting that the lowest transition energy is estimated using an emission band, which is higher in energy than the lowest energy UV−vis absorption band. Such an anti-Kasha emission seems implausible, perhaps indicating that the observed emission may originate from an emissive decomposition product instead of the excited radical itself, which leads to an overestimation of the excited state redox potential of Mes-Acr$^{\bullet}$ and possibly to a complete mechanistic misinterpretation.

Donor−acceptor cyanoarenes such as 4-DPAIPN (2,4,5,6-tetrakis(diphenylamine)isophthalonitrile) and 3CzEPAIPN (2,4,5-tri(9H-carbazol-9-yl)-6-(ethyl(phenyl)amino)-isophthalonitrile) are strong photoreductants in their excited radical anion forms. In the case of 3CzEPAIPN (Table 1, entry 12), electron-rich aryl-chlorides with reduction potentials as negative as −2.9 V versus SCE were reduced using a ConPET excitation strategy (Figure 2k). Excited 4-DPAIPN$^{\bullet-}$ exhibits even more extreme reduction power (Table 1, entry 13), regardless of the excitation strategy employed (ConPET or e-PRC).[20,57] Using a ConPET excitation strategy, electron-poor aryl-chlorides with reduction potentials as low as −3.4 V versus SCE could be activated and trapped with various reagents such as P(OEt)$_3$ or B_2pin_2 in yields ranging from 70% to 92% (Figure

https://doi.org/10.1021/jacsau.4c00974
JACS Au 2025, 5, 426−447

Table 2. Summary of Selected Key Properties of Known Reactive Excited Organic Radical Cations and the Corresponding Precursor Compounds

	$PC^{\bullet+}$	$E(PC^{\bullet+}/PC)$/V vs SCE	E_{D1}/eV[a]	τ_{D1}/ps	$E(^2*PC^{\bullet+}/PC)$/V vs SCE calc.[b]	$E(^2*PC^{\bullet+}/PC)$/V vs SCE obs.[c]	applications
1	$PTZ^{\bullet+}$	0.6[85]	1.4[85]	n/a	2.0	1.5[d]	Bimolecular [1 + 4] cyclization or [1,2] addition of 1,1-diphenylethylene.[85]
2	$TPPD^{\bullet+}$	0.7[87]	1.6[97]	n/a	2.2	1.9[e]	Oxidation reaction of benzyl alcohol to benzaldehyde.[87]
3	$TpBPA^{\bullet+}$	0.9[25]	1.3 (D_1)[25]	n/a	2.2 (D_1)	2.2[f]	C−H heteroamination reaction of electron-rich arenes.[25]
			3.1 (D_2)[25]		4.0 (D_2)		
4	$TPAC(Me)_2^{\bullet+}$	0.7[92]	1.5[92]	~10[92]	2.2	2.4[g]	C−H heteroamination of electron-deficient arenes.[92]
5	$PTH^{\bullet+}$	0.9[5]	1.3[5]	36[8]	2.2	2.5[h]	C−H heteroamination of electron deficient arenes.[6] Pentafluorosulfanylation reaction of α-methyl- and α-phenylstyrene using SF_6.[7,42,86] Chloride anion oxidation reaction.[5]
6	$TCBPA^{\bullet+}$	1.0[25]	1.4 (D_1)[25]	n/a	2.4 (D_1)	2.3[i]	C−H heteroamination of arenes.[25]
			3.2 (D_2)[25]		4.2 (D_2)		
7	$TdCBPA^{\bullet+}$	1.3[25]	1.4 (D_1)[25]	n/a	2.7 (D_1)	≥3.0[j]	C−H heteroamination of highly electron-deficient arenes.[25]
			3.1 (D_2)[25]		4.4 (D_2)		
8	$TAC^{\bullet2+}$	1.3[4]	2.0[4]	n/a	3.3	2.4[k]	C−H functionalization of electron-deficient arenes.[4] Acetoxyhydroxylation reaction of aryl olefins.[81] C−H functionalization reaction of ethers.[82] Aminooxygenation reactions of aryl olefins.[83] Diamination and oxyamination reactions of vicinal C−H bonds.[1] Oxygenation of multiple adjacent C−H bonds.[84]

[a]The lowest doublet excited state energies (E_{D1}) were estimated by taking the point on the low-energy side of the absorption spectra of the photocatalysts, at which 10% of the maximum absorption is reached. The higher doublet excited state energies (E_{D2}) were estimated by taking the point on the low-energy side of the second absorption band, at which 10% of the maximum absorption is reached. [b]The excited state redox potentials ($E(^2*PC^{\bullet+}/PC)$) were calculated using the Rehm−Weller equation $E(^2*PC^{\bullet+}/PC) \approx E(PC^{\bullet+}/PC) + E_D \times e$, with the elementary charge e, the ground state potentials ($E(PC^{\bullet+}/PC)$, column 3), and the D_1 energy or D_2 energy (E_D, column 4). [c]Determined by analyzing the substrate with the lowest oxidation potentials. [d]Estimated from 1,1-diphenylethylene.[98] [e]Estimated from benzylalcohol.[88] [f]Estimated from bromobenzene.[4] [g]Estimated from 1,4-dichlorobenzene.[4] [h]Estimated from benzene.[6] [j]Estimated from chlorobenzene.[4] [i]Estimated from α,α,α-trifluorotoluene and 1,2,4-trifluorobenzene.[25] [k]Estimated from 1,3-dichlorobenzene.[4]

2k). Furthermore, cleavage of C—N bonds in cyclic amines was accomplished, forming amino acids in the presence of CO_2 (Figure 2l). When utilizing an e-PRC excitation strategy, cleavage of strong aryl C−N and C−O bonds to form aryl radical intermediates was attained, with yields ranging from 40% to 98% (Figure 2j).[20,57] Evidently, substrates requiring potentials as negative as −3.4 V versus SCE were activated, which is difficult to rationalize based on the theoretical excited state potential of −3.1 V versus SCE for $4\text{-DPAIPN}^{\bullet-}$.

The 4,4′-dicyanobiphenyl radical anion ($DCB^{\bullet-}$) is an extremely strong photoreductant, capable of initiating base-promoted homolytic aromatic substitution (BHAS) (Figure 2m) and intramolecular radical nucleophilic substitution reaction of 2-halide-*N*-phenylanilines to carbazole.[38] Due to the absence of a visible absorption band in the precursor photocatalyst (DCB), a ConPET excitation strategy with a second chromophore was employed to enable visible light-driven catalysis (Figure 1b). This catalytic system was successfully applied to activate $C(sp^2)$—Cl and $C(sp^2)$—F bonds, requiring reduction potentials of down to −3.0 V versus SCE, matching the theoretically available potentials of −3.2 V versus SCE.[38]

3.2. Oxidative Catalysis Using Excited Organic Radicals

Organic radical cations, serving as potent photo-oxidants, have been less frequently studied than excited organic radical anions. This difference may arise from the availability of numerous electron donors compared to fewer electron acceptors.[6] Hence, most excited organic radical cations are generated using the e-PRC strategy.[1,4,6,25,81−85] The few ConPET excitation strategy examples often incorporate the used electron acceptor into their final product.[7,42,86] In the following, photocatalytic systems employing organic radical cations are considered and ordered along their calculated theoretical excited state oxidation potential (Table 2). In cases where the organic radical cationic photocatalyst could be successfully used for catalysis requiring oxidation potentials more positive than the calculated theoretical value, the deviation is marked by a gray hatched areas in Figure 3a.

In 1979, an electrochemically mediated photoredox strategy was employed on phenothiazine (PTZ) to generate the excited phenothiazine radical cation ($^2*PTZ^{\bullet+}$).[85] This species was utilized to oxidize diphenylethylene to form 1,1,4-triphenyl-1,2-dihydronaphthalene and 2,2,5,5-tetraphenyl-tetrahydrofuran (Figure 3b). This reaction requires an oxidation potential of +1.5 V versus SCE, which is substantially lower than the calculated $^2*PTZ^{\bullet+}$ oxidation potential of +2.0 V versus SCE (Table 2, entry 1). Whether or not $PTZ^{\bullet+}$ reacts catalytically in this initial example remained unclear.[85] The same research group excited the electrochemically generated *N*,*N*,*N*′,*N*′-tetraphenyl-*p*-phenylenediamine radical cation ($TPPD^{\bullet+}$) with UV light to achieve the oxidation reaction of benzyl alcohol to benzaldehyde (Figure 3j) with a turnover number (TON) of 3.[48,87] Benzyl alcohol oxidation typically requires redox potentials of ~ +1.9 V versus SCE,.[88] In contrast, the calculated oxidation potential for excited $TPPD^{\bullet+}$ is ~ +2.2 V versus SCE (Table 2, entry 2). Other early studies demonstrated the photoreactivity of radical cations in stoichiometric amounts,[89−91] but subsequently, it took almost half a century until excited radical cations regained attention as possible

https://doi.org/10.1021/jacsau.4c00974
JACS Au 2025, 5, 426−447

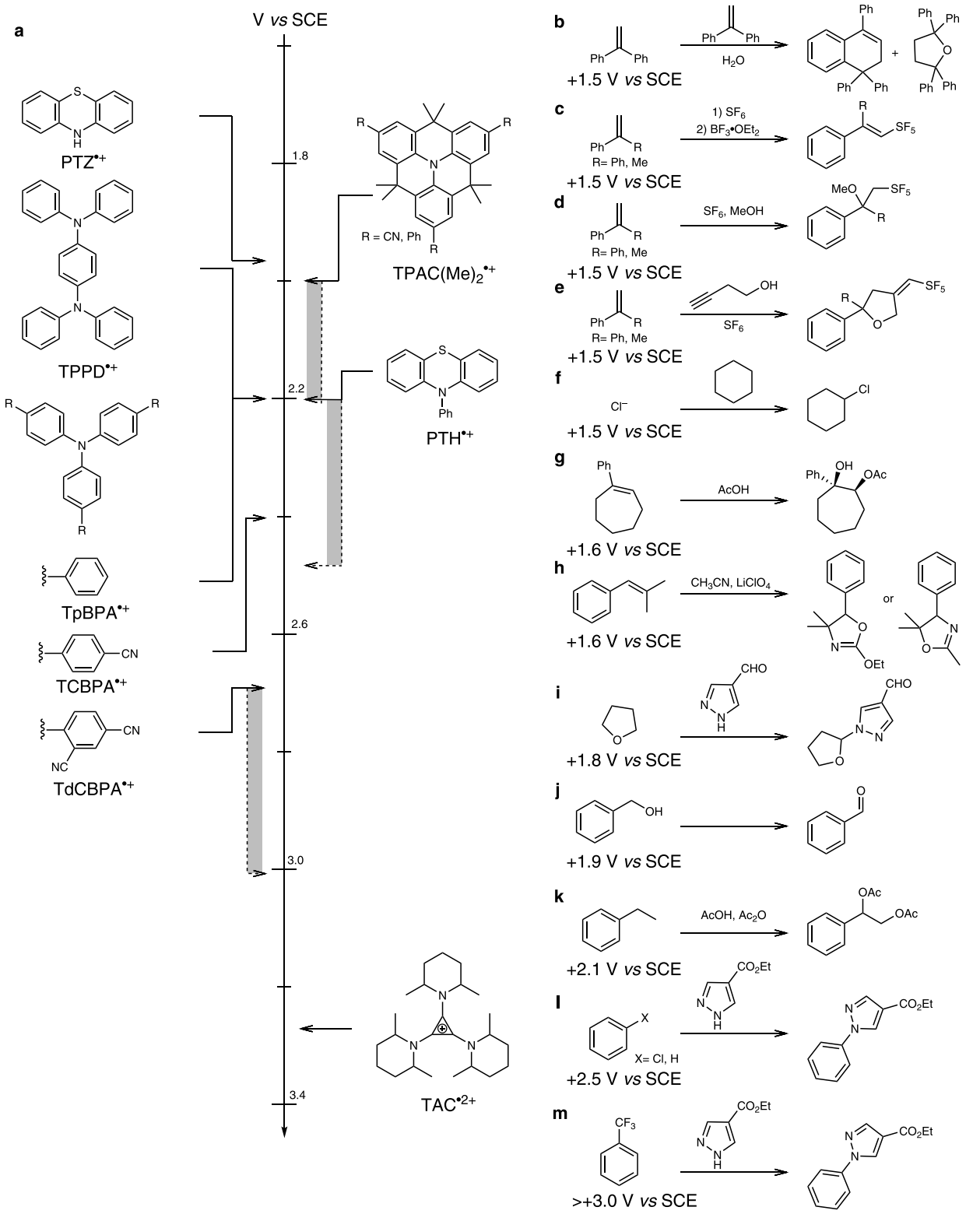

Figure 3. a. Excited state oxidation potentials of various radical cations as determined using the Rehm−Weller equation. In cases where the observed reactivity surpasses the theoretical oxidation potential, the gray hatched regions highlight the deviation to the oxidation potentials of activatable substrates. **b.** Bimolecular cyclization reaction of 1,1-diphenylethylene.[85] **c−e.** Pentafluorosulfanylation of α-methyl- and α-phenylstyrene using SF_6.[7,42,86] **f.** Chloride oxidation reaction.[5] **g.** Acetoxyhydroxylation reaction of aryl-olefins.[81,95] **h.** Diamination and oxyamination reactions of vicinal C—H bonds.[1] **i.** Regioselective C—H functionalization of ethers. **j.** Oxidation reaction of benzyl alcohol to benzaldehyde.[87] **k.** Oxygenation reaction of multiple adjacent C—H bonds.[84,96] **l.** Oxidative activation of electron-deficient arenes.[4,6,25,92] **m.** Oxidative activation of α,α,α-trifluorotoluene.[25]

photocatalysts,[4] using structurally similar compounds such as *N*-phenyl-phenothiazine[5−7,42,86] or diphenylamine derivatives.[25,92]

Using an e-PRC excitation strategy, tri(biphenyl-4-yl)amine derivatives (TpBPA, TCBPA, TdCBPA, Figure 3a) could be applied to activate electron-deficient arenes for C—H or

https://doi.org/10.1021/jacsau.4c00974
JACS Au 2025, 5, 426−447

electron-deficient fluoroarenes for C—F functionalization with 1H-pyrazole derivatives (Figure 3l/m). Depending on the functionalization of the tri(biphenyl-4-yl)amines, different excited state redox potentials between +2.2 and +2.7 V versus SCE were calculated, which contrasts with the observed reactivity of substrates requiring potentials > +3.0 V versus SCE (Figure 3m). DFT calculations suggested that the biphenyl units of TpBPA, TCBPA, TdCBPA enable better preassociation with substrate molecules than single phenyl units, and the authors speculated that anti-Kasha reactivity from an ultrashort-lived higher excited state (Table 2, entry 7) could occur.[25] This would rationalize the observed reactivity, as potentials up to +4.4 V versus SCE could be reachable by anti-Kasha behavior (Table 2, entries 3, 6, and 7).

Chemically interlocked triarylamine derivatives (TPAC-$(Me)_2$, Figure 3a) were also investigated. Their more planar geometry was hypothesized to improve the preassociation of substrate molecules via cation-π interaction. The interlocked phenyl units may also extend the radical cation's excited state lifetime, as the aromatic rings' rotation often facilitates excited state relaxation.[93] The authors further anticipated higher photostability, although the more planar structure could make these compounds more prone to electrophilic attack, similar to what is observed for square planar transition metal complexes.[94] By employing oxygen as an electron acceptor and 400 nm light irradiation, a ConPET excitation strategy was used to generate the highly oxidative $^{2*}[TPAC(Me)_2]^{\bullet+}$ species for the oxidation of benzene. The resulting phenyl radical cation could be trapped using ethyl 1H-pyrazole-4-carboxylate (Figure 3l). However, only yields of ∼6% were observed. Therefore, the authors added $SbCl_5$, a strong oxidant in catalytic amount for the *in situ* generation of the photoactive $TPAC(Me)_2^{\bullet+}$, leading to yields of 88%. This enabled the activation of electron-deficient arenes for C—H functionalization and activated electron-deficient fluoroarenes for C—F functionalization with 1H-pyrazole derivatives. These reactions usually require oxidation potentials of ∼ +2.4 V versus SCE. This is slightly higher than the calculated oxidation potential of ∼ +2.2 V versus SCE for $^{2*}[TPAC-(Me)_2]^{\bullet+}$. Interestingly, only product traces were reported for any triarylamine photocatalyst when employing an e-PRC strategy using red light, to excite into the lowest excited state, which could indicate the need for anti-Kasha behavior.

N-phenyl-phenothiazine (PTH) and its derivatives represent another class of photosensitizers used for their highly oxidative properties in the doublet excited state ($^{2*}PTH^{\bullet+}$).[5−7,42,86] One research group employed a ConPET excitation strategy using UV light for the catalytic pentafluorosulfanylation of α-substituted alkenes.[7,42,86] Upon UV light excitation, phenothiazine's strong excited state reduction potential enables the activation of challenging substrates such as SF_6, leading to the formation of $PTH^{\bullet+}$ with an oxidation potential of +0.6 V versus SCE and $SF_6^{\bullet-}$, which subsequently fragments into $SF_5^{\bullet}$ and F^-. Upon photoexcitation with a second UV photon, $^{2*}PTH^{\bullet+}$ is formed, activating styrene derivatives with oxidation potentials of approximately +1.5 V versus SCE. The resulting benzyl radical cations were trapped by the $SF_5^{\bullet}$, ultimately forming a vinylic SF_5 functional group after additional treatment with $BF_3{\cdot}OEt_2$ (Figure 3c).[42]

When adding MeOH to the reaction, the formed benzylic radical is first captured by MeOH, followed by pentafluorosulfanylation by the remaining $SF_5^{\bullet}$ (Figure 3d).[7] Similarly, in the presence of 3-butynol, an analogous ether intermediate is formed, but eventually, intramolecular cyclization occurs, followed by recombination with $SF_5^{\bullet}$, resulting in the product in Figure 3e.[86] The oxidizing $PTH^{\bullet+}$ species can also be generated via 390 nm excitation of PTH followed by one-electron oxidation by oxygen. Upon a second UV photon absorption, the doublet excited state ($^{2*}PTH^{\bullet+}$) is formed, activating benzene derivatives. The formed aryl cation can be trapped using 1H-pyrazole derivatives (Figure 3). The same excitation strategy using oxygen as an electron acceptor was used to oxidize chloride anions, which usually requires ∼ +1.5 V versus SCE. The formed chloride radical could be used to chlorinate unactivated $C(sp^3)$—H bonds, such as in cyclohexane (Figure 3f).[5] Despite the wide variety of reactions, $^{2*}PTH^{\bullet+}$ only exhibits a calculated maximum oxidation potential of approximately +2.2 V versus SCE. Surprisingly, reactions of substrates requiring potentials of up to +2.5 V versus SCE were achieved.

The trisaminocyclopropenium radical dication ($TAC^{\bullet2+}$) was broadly used in e-PRC studies.[39] Using a 23 W compact fluorescent light, benzyl derivatives were oxidized and trapped by 1H-pyrazole derivatives (Figure 3). Using the same methodology, $TAC^{\bullet2+}$ was employed for regioselective C—H functionalization of ethers (Figure 3i),[82] acetoxyhydroxylation of aryl olefins (Figure 3g),[81] diamination and oxyamination of vincinal C—H bonds,[1] aminooxygenation of aryl olefins (Figure 3h)[1,83] and oxygenation of multiple adjacent C—H bonds (Figure 3k).[84] Here, an excited state oxidation potential of +3.3 V versus SCE was calculated. Despite this extreme theoretical oxidation potential, photocatalytic reactions with α,α,α-trifluorotoluene, which requires an oxidation potential of +3.0 V versus SCE, could not be observed.

4. MECHANISTIC INVESTIGATIONS OF EXCITED RADICALS

Despite the demonstrated applications of organic radicals in synthetically oriented photoredox catalysis, the reaction mechanisms have remained largely unclear. In many cases, it is uncertain whether the excited organic radicals are truly the active species in the photocatalytic process. One reason for doubt is that the observed chemical reactivity in many cases implies redox potentials significantly beyond the expected values of the respective excited organic radicals (see discussion above and Figures 2 and 3). These discrepancies between expected and observed reactivity suggest the involvement of alternative primary mechanisms, such as the *in situ* generation of photoactive decomposition products with more potent redox potentials.[29,76] Another possibility is the underestimation of the excitation energies of the radicals, leading to underestimated excited state redox potentials. However, this scenario would necessitate reactivity from higher excited states, which typically undergo internal conversion to the lowest excited state within <100 fs following Kasha's rule.[99] It is currently believed that such short excited state lifetimes are orders of magnitude too short for photoinduced electron transfer, even when preassociation between organic radicals and substrate molecules is considered.[32−35]

In the following, we summarize mechanistic studies involving photoactive excited radical ions to explore the primary mechanism, whereas discussion of key spectroscopic and analytical techniques can be found in other review articles.[100−103] Given the relative scarcity of such studies, structurally similar photocatalysts are collectively analyzed. This direct comparative approach leads to mechanistic insight even

https://doi.org/10.1021/jacsau.4c00974
JACS Au 2025, 5, 426−447

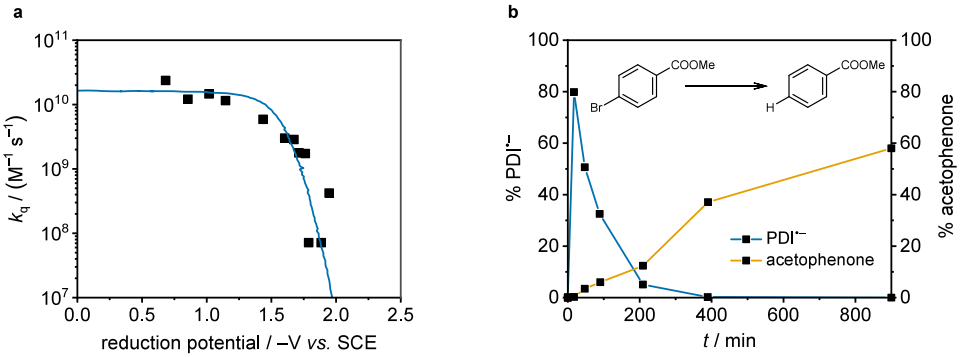

Figure 4. a. Rehm–Weller analysis of the diffusion-based rate constant for photoinduced electron transfer from excited $PDI^{\bullet-}$ against the reduction potentials of various electron acceptors. The blue trace represents the calculated fit according to the Rehm–Weller model.[35] Raw data were extracted[106] from ref.[35] **b.** Yield for the reaction of 4-bromoacetophenone to acetophenone (orange trace) and relative percentage of $PDI^{\bullet-}$ present (blue trace) as a function of irradiation time.[30] Raw data were extracted[106] from ref.[30]

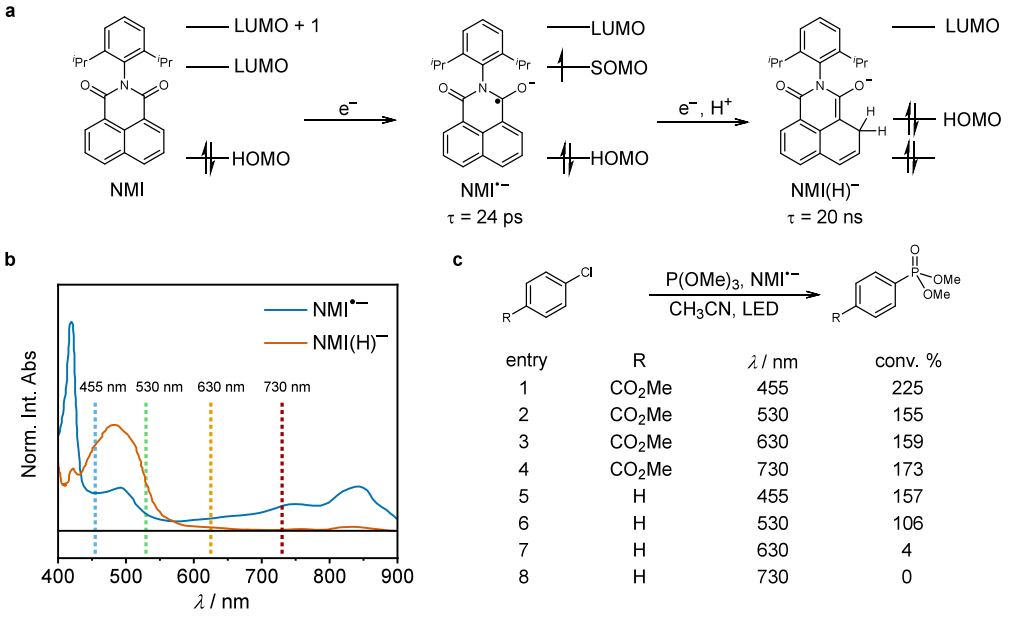

entry	R	λ / nm	conv. %
1	CO_2Me	455	225
2	CO_2Me	530	155
3	CO_2Me	630	159
4	CO_2Me	730	173
5	H	455	157
6	H	530	106
7	H	630	4
8	H	730	0

Figure 5. a. Single electron reduction of naphthalene monoimide (NMI) to the radical anion ($NMI^{\bullet-}$) with a doublet excited state lifetime of 24 ps. Following a second electron transfer and protonation, an emissive Meisenheimer complex ($[NMI(H)]^-$) with a singlet excited state lifetime of 20 ns is formed.[29] **b.** Normalized absorption spectra of the NMI radical anion (solid blue trace) and the Meisenheimer complex (solid orange trace).[29] Raw data were extracted[106] from ref.[29] **c.** Conversion of aryl-chloride derivatives to dimethylphenylphosphonates (relative to the used internal standard) using quantitative ^{31}P NMR spectroscopy after excitation at different wavelengths (λ, as marked by vertical dotted lines in b) using chemically generated $NMI^{\bullet-}$ in stoichiometric amounts.[24]

for radical ions that so far have not been studied in mechanistically oriented work.

4.1. Radical Anions

Polyaromatic Imide Radical Anions. Polyaromatic imides are widely used precatalysts to form the corresponding radical anion, initiating the photocatalysis upon excitation (Figure 2).[21,22,24,28,59−62,65,66] However, this class of radical anion photocatalysts shows reactivity beyond their expected limits set by the radical anion excited state potential (Table 1). The ^{2}*$PDI^{\bullet-}$ reactivity was examined using ultrafast UV–vis transient absorption (TA) spectroscopy to experimentally determine the radical anion's excited state redox potential.[35] $PDI^{\bullet-}$ was chemically generated, and upon excitation into the lowest excited state, UV–vis TA spectroscopy revealed a D_1 excited state lifetime of 160 ps in solution at room temperature. A decrease in the excited state lifetime was observed in the presence of various aromatic electron acceptors, and Stern–Volmer analysis provided the diffusion-based bimolecular electron transfer rate constants for these electron acceptors. The Rehm–Weller analysis of the electron transfer rate constant and the reduction potentials of various electron acceptors resulted in an oxidation potential of −1.87 V versus SCE for D_1-excited $PDI^{\bullet-}$ (Figure 4a).[49,104,105] This value represents the experimentally measured excited state redox potential, which falls within the uncertainty margin of the calculated excited state reduction potential of −1.7 V versus SCE.[35] Surprisingly, dynamic quenching for 4-bromoacetophenone was unobservable in the UV/vis TA study, even though this substrate was employed in photoredox catalysis using $PDI^{\bullet-}$ as a photocatalyst,[22] indicating a bimolecular reaction rate constant of $<1 \times 10^8$ M^{-1} s^{-1}. This, in turn, implies a maximum electron transfer efficiency of ∼0.3% from the excited $PDI^{\bullet-}$ to 4-bromoacetophenone for the relevant concentration of 4-bromoacetophenone (170 mM) and the natural D_1-excited

https://doi.org/10.1021/jacsau.4c00974
JACS Au 2025, 5, 426−447

state lifetime of $PDI^{\bullet-}$ (160 ps).[22] Such a low reaction efficiency seems an unrealistic driver of the observable photochemistry considering the usage of a low-power LED, the comparatively short reaction time (3 h), and the product yield of 82% obtained in the initial synthetically oriented study.[22] To understand these peculiarities, the reaction progress of 4-bromoacetophenone to acetophenone was monitored over time (Figure 4b).[30] This study used UV−vis absorption spectroscopy to track the relative concentration of $PDI^{\bullet-}$ over a reaction period of 900 min using 450 nm light excitation. The UV−vis absorption signal of $PDI^{\bullet-}$ at 950 nm increased during the initial 20 min but declined after a longer irradiation time (Figure 4b). In contrast, product formation was relatively slow during the first 20 min of the reaction, where a high concentration of the proposed photoactive $PDI^{\bullet-}$ was present. However, as irradiation progressed and the concentration of $PDI^{\bullet-}$ decreased, the rate of product formation accelerated. Collectively, these findings quite clearly indicate that $PDI^{\bullet-}$ cannot act as the catalyst upon 450 nm excitation for the reduction of 4-bromoacetophenone, and the authors concluded that an in situ formed photodecomposition product is likely to act as the photocatalyst in this case. However, identifying the photoactive decomposition products of $PDI^{\bullet-}$ remained unsuccessful. Nevertheless, this study revealed that decomposition only occurs in the presence of 4-bromoacetophenone, leading to the appearance of a new paramagnetic species.

A recent study utilized various red light-absorbing photosensitizers to generate the proposed photoactive $PDI^{\bullet-}$ via a triplet-mediated ConPET excitation strategy.[46] In this mechanism, a photosensitizer is excited, reaching a triplet excited state. A subsequent triplet−triplet energy transfer to PDI generates ^{3}PDI. In the presence of an electron donor, the triplet excited state is reductively quenched, forming the claimed photocatalyst $PDI^{\bullet-}$. This catalytic system enables the use of 650 nm light irradiation, compared to 450 nm without a photosensitizer, while maintaining comparable reactivity with similar reaction times and low-power LEDs. This paves the way for larger-scale photocatalytic reactions and potential biological applications.[46] However, as photostability in the presence of 4-bromoacetophenone was not investigated, it remains unclear whether the unknown decomposition product also absorbs red light or if sensitized ConPET remains the dominant mechanism with this specific excitation strategy. This uncertainty is underscored by a related study on naphthalene diimide (NDI), where complete decomposition of $NDI^{\bullet-}$ was observed after 25 min of irradiation in the presence of 4-bromobenzonitrile.[66] As a result, this study also suggested the presence of a photoactive decomposition product, however, the specific photoactive degradation product remained unidentified.[66]

A recent study into the structurally related naphthalene monoimide precatalyst (NMI, Figure 5a) provided insight into the possible nature of the observed photoactive decomposition products of $NMI^{\bullet-}$ and $PDI^{\bullet-}$. This study found that the photoactive species might not be the NMI radical anion ($NMI^{\bullet-}$) with its excited state lifetime of 24 ps, but rather a two-electron reduced and protonated, closed shell Meisenheimer complex ($[NMI(H)]^-$) with a significantly longer excited state lifetime of 20 ns (Figure 5a). Using UV−vis spectroelectrochemistry, the authors identified both $NMI^{\bullet-}$ and $[NMI(H)]^-$ species (Figure 5b) and determined their excited state redox potential to be approximately −2.7 V versus SCE in both cases. However, the 3 orders of magnitude longer excited state lifetime of the closed-shell Meisenheimer complex $[NMI(H)]^-$ makes diffusion-controlled redox reactions far more kinetically competitive with the inherent excited-state deactivation pathway compared to ^{2}*$NMI^{\bullet-}$. A Stern−Volmer analysis resulted in a rate constant of 3×10^9 M^{-1} s^{-1} for SET from the Meisenheimer complex ($[NMI(H)]^-$) to 4-methylchlorobenzoate and a rate constant of 1×10^7 M^{-1} s^{-1} in the case of chlorobenzene, which is a compelling evidence for the photoredox activity of the Meisenheimer complex.

In an alternative approach to understanding the reaction mechanism, $NMI^{\bullet-}$ was chemically generated and isolated using KC_8 to investigate its photocatalytic reactivity.[24] Utilizing $NMI^{\bullet-}$ species as a photoreductant in stoichiometric amounts, they explored the photoreactivity as a function of excitation wavelengths (Figure 5c). When using methyl 4-chlorobenzoate with a redox potential of −2.0 V versus SCE as a substrate,[107] conversions (relative to the used internal standard) of 225% (at 455 nm), 155% (at 530 nm), 159% (at 630 nm), and 173% (at 730 nm) were observed (Figure 5c, entry 1−4). These results are consistent with the absorption spectrum of $NMI^{\bullet-}$ (Figure 5b, blue line), which displays a strong absorption across all applied wavelengths. Furthermore, these results align with the calculated excited-state reduction potential of −2.7 V versus SCE for D_1-excited $NMI^{\bullet-}$. However, when chlorobenzene with a redox potential of −2.8 V versus SCE was employed as a substrate,[108] significant conversions were exclusively observed when using either 455 nm (157%) or 530 nm (106%) light excitation (Figure 5c, entries 5−8). These findings align more closely with the UV−vis absorption spectrum of the Meisenheimer complex (Figure 5b), even though the authors could not detect its formation. But, in the initial mechanistic study, the Meisenheimer complex did undergo dynamic excited-state quenching with chlorobenzene, suggesting the formation of $[NMI(H)]^-$ under these catalytic conditions.[29] However, neither the formed Meisenheimer complex nor the $NMI^{\bullet-}$ can explain the observed reactivity of extremely inert substrates, such as 1,3-di-*tert*-5-chloro-2-methoxybenzene, which has a reduction potential of −3.4 V versus SCE.[28] Both potentially photoactive species exhibit significantly lower excited-state potentials.

A possible explanation can be found in the mechanistic study of the structurally related benzo[*ghi*]perylene monoimide precatalyst (Figure 6a).[76] This proposed photoactive precatalyst was applied for a photoinduced Birch reduction of benzene, requiring reduction potentials of −3.4 V versus SCE (Figure 2n).[13] Initially, reactivity was attributed to the excited radical anion,[13] similar to $PDI^{\bullet-}$ and $NMI^{\bullet-}$ discussed above.[21,22,24,28,59−62,65,66] A recent study including the same research group uncovered the possibility of an imide ring opening reaction under reaction conditions (Figure 6c).[13] The authors identified BPI-RO (Figure 6d) as the most plausible photoactive decomposition product. Due to the instability of the BPI-RO intermediate, a model photocatalyst was employed for the mechanistic investigation (Figure 6b), representing the ring-opened species. Using this model compound, they observed reactivity from an emissive doubly reduced and protonated intermediate (Figure 6d),[76] similar to the above-discussed Meisenheimer complex.[29] The emission of the reactive intermediate (Figure 6d) could be quenched by adding benzene, resulting in a Stern−Volmer constant (K_{SV}) of 0.39 M^{-1}. This study convincingly demonstrates that the photoactive species may also arise from a more complex photodegradation product. Hence, a similar decomposition product could perhaps explain

https://doi.org/10.1021/jacsau.4c00974
JACS Au 2025, 5, 426−447

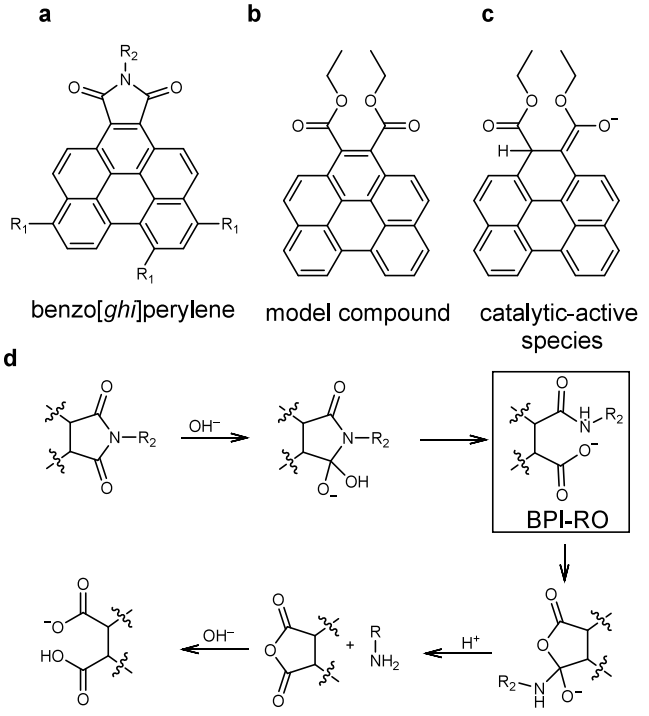

Figure 6. a. Used catalyst for the photoinduced Birch reduction of benzene.[13] **b.** Model compound for the ring-opened precursor photocatalyst. **c.** Proposed photoactive Meisenheimer complex of the model compound. **d.** Proposed ring opening decomposition pathway of the precursor compound.[76]

the observed reactivity of ^{2}*NMI$^{\bullet-}$ with 1,3-di-*tert*-butyl-5-chloro-2-methoxybenzene.[13]

To summarize this section on polyaromatic diimides, our simple analysis indicates the possibility of different main reaction pathways depending on the involved substrates or used excitation wavelength. This could be due to differences in preassociation strength, the formation of different decomposition products, variations in reaction rate constants, or even reactions from higher excited states (anti-Kasha reactivity). Overall, most mechanistic studies investigating the photoredox activity of polyaromatic imide radical anions strongly suggest that decomposition products are often responsible for the observed photoreactivity. This relatively new insight into photodegradation products could pave the way for designing novel closed shell photocatalysts with extremely high excited-state redox potentials,[13,29,109,110] showing the importance of such mechanistic investigations.

Dicyanoarene Radical Anions. 9,10-Dicyanoanthracene radical anion (DCA$^{\bullet-}$) is a widely used compound for ConPET and e-PRC (Figure 7a).[10,24,27,43,71] However, the limited stability and the observed photoreactivity of DCA$^{\bullet-}$, which in some cases exceeds its predicted reduction power significantly, raise doubts about whether DCA$^{\bullet-}$ is really the photoactive species driving the catalysis.[29,33]

Earlier investigations attributed strong fluorescence emission centered around 500 nm to ^{2}*DCA$^{\bullet-}$, suggesting a transition energy of approximately 2.4 eV and an excited state lifetime of 12.5 ns.[111,112] However, recent studies have revealed a much shorter excited state lifetime of 3 ps,[33] and a lower transition energy of 1.7 eV,[10,43] resulting in a lower excited state reduction potential of −2.6 V versus SCE. Further, the observed emissive species was identified as the 10-cyanoanthrolate anion formed through the reaction of DCA$^{\bullet-}$ with oxygen.[29,90,113] Nowadays, anthrolates are recognized as potent photocatalysts with absorption bands between 400 and 550 nm (Figure 7c, blue trace).[114,115] This can be problematic, as many synthetically oriented studies employ blue or green light to generate ^{2}*DCA$^{\bullet-}$. In the presence of trace amounts of oxygen, the photoactive 10-cyanoanthrolate anion degradation product can be formed and is then excited efficiently with light of these wavelengths.[10,27,43,71]

To minimize the risk of exciting 10-cyanoanthrolate anion or other photoactive decomposition products, a recent study employed $[Cu(dap)_2]^+$ as a photosensitizer to generate the proposed photocatalytically active DCA$^{\bullet-}$ using red light (635 nm).[43] Upon absorption of a second red photon, SET from ^{2}*DCA$^{\bullet-}$ activates a selection of 50 substrates, with reduction potentials ranging from −1.8 V versus SCE to −2.6 V versus SCE (Figure 7b). This ConPET approach with two different chromophores avoids the need for blue or green light excitation, which might otherwise excite photoactive decomposition products (Figure 7c). Further, no reactivity requiring stronger reduction potential was observed than indicated by the calculated potential limit of ^{2}*DCA$^{\bullet-}$ (−2.6 V versus SCE).

A mechanistically oriented study utilized a similar approach, using chemically generated DCA$^{\bullet-}$ in stoichiometric amounts to activate different aryl chlorides (Figure 7d) across various excitation wavelengths.[24] For methyl 4-chlorobenzoate with a reduction potential of −2.0 V versus SCE,[107] reactivity was observed across all applied wavelengths (Figure 7d, entries 1−4). The conversions (relative to the used internal standard) of 247% (at 455 nm), 82% (at 530 nm), 77% (at 630 nm), and 37% (at 730 nm) align well with the UV−vis absorption spectrum of DCA$^{\bullet-}$ (Figure 7c, orange trace) with strong absorption features at all applied wavelengths. In contrast, the resulting conversions do not align with the absorption spectrum of the proposed decomposition product, 10-cyanoanthrolate anion, which shows no absorption above 550 nm (Figure 7c, blue trace). However, when chlorobenzene, with a redox potential of −2.8 V versus SCE[108] was tested, conversions of 174% (at 455 nm), 3% (at 530 nm), 0% (at 630 nm), and 0% (at 730 nm) were observed (Figure 7d, entries 5−8). The lack of conversion with 630 and 730 nm light excitation, as well as the required high reduction potential contrasts with the UV−vis absorption spectrum of DCA$^{\bullet-}$ and the expected reduction power of excited DCA$^{\bullet-}$. Conversely, the UV−vis absorption spectrum of 10-cyanoanthrolate anion is in relatively good agreement with the observed excitation wavelength-dependent conversion. However, anthrolate anions typically possess reduction potentials of −2.5 V versus SCE,[114,115] which should be insufficient to activate chlorobenzene.

Speculatively, a doubly reduced and protonated DCA species ($[DCA(H)]^-$), similar to what has been observed for NMI (see discussion above), could be the photoactive species (Figure 7a). This hypothesis appears plausible, considering the excess (1.1 equiv) of the KC_8 reductant agent used, with a potential of −1.8 V versus SCE.[117] This potential would be sufficient to generate the doubly reduced DCA species with a reduction potential of approximately −1.6 V versus SCE,[43] and proton-coupling is expected to further facilitate this 2-fold reduction event. The UV−vis absorption spectrum of $[DCA(H)]^-$ (Figure 7c) shows spectral features from 455 to 595 nm (corresponding to >2.0 eV), resulting in an estimated excited state redox potential of approximately −3.6 V versus SCE, sufficient for the observed reactivity.[27] However, the UV−vis absorption signals observed

https://doi.org/10.1021/jacsau.4c00974
JACS Au 2025, 5, 426−447

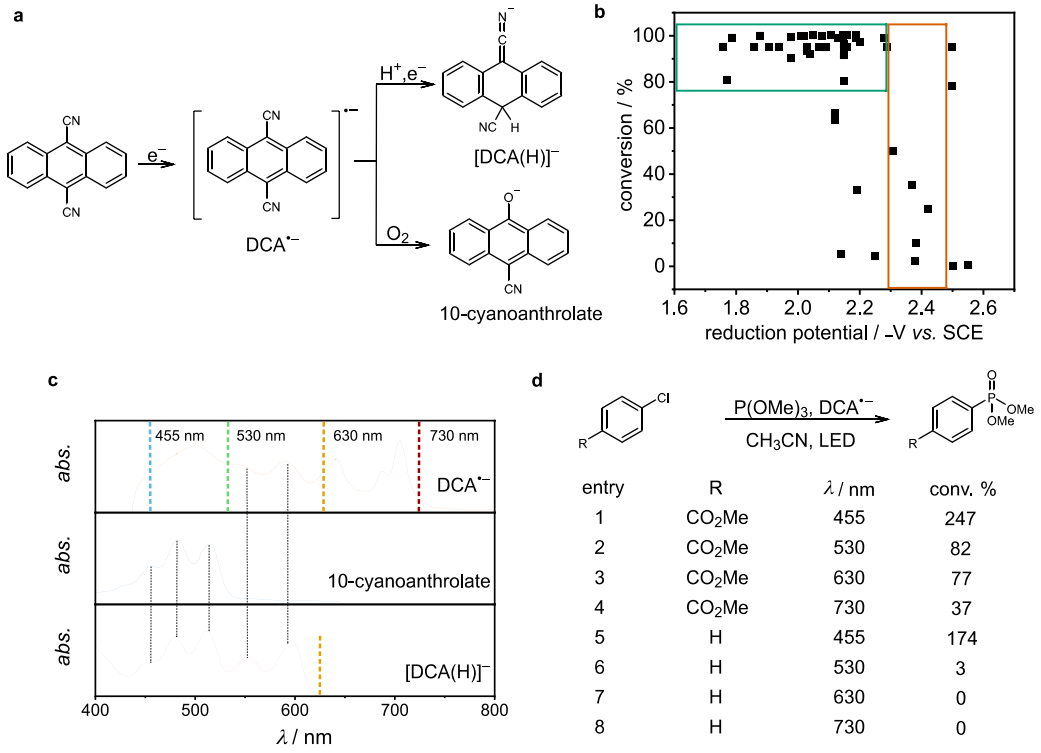

entry	R	λ / nm	conv. %
1	CO_2Me	455	247
2	CO_2Me	530	82
3	CO_2Me	630	77
4	CO_2Me	730	37
5	H	455	174
6	H	530	3
7	H	630	0
8	H	730	0

Figure 7. a. Formation of the 9,10-dicyanoanthracene radical anion ($DCA^{\bullet-}$) and the photodegradation products 10-cyanoanthrolate anion and the doubly reduced and protonated 9,10-dicyanoanthracene ($[DCA(H)]^-$). **b.** Obtained substrate conversion yields for dehalogenation and detosylation reactions against the reduction potential of 50 tested substrates. For these red-light driven reactions, almost all substrates with a reduction potential less negative than −2.3 V lead to 80% or higher conversion (green box), whereas substrates with more negative potentials (red box) lead to lower conversions. Data was extracted[106] from ref.[43] **c.** UV−vis absorption spectrum of $DCA^{\bullet-}$,[43] 10-cyanoanthrolate,[116] and the doubly reduced and protonated dicyanoanthracene ($[DCA(H)]^-$).[27] Raw data was extracted[106] from the corresponding refs[27,43,116] **d.** Conversion of aryl chloride derivatives to dimethylphenylphosphonates determined by quantitative ^{31}P NMR spectroscopy using different excitation wavelengths (λ) and chemically generated $DCA^{\bullet-}$ in stoichiometric amounts.[24]

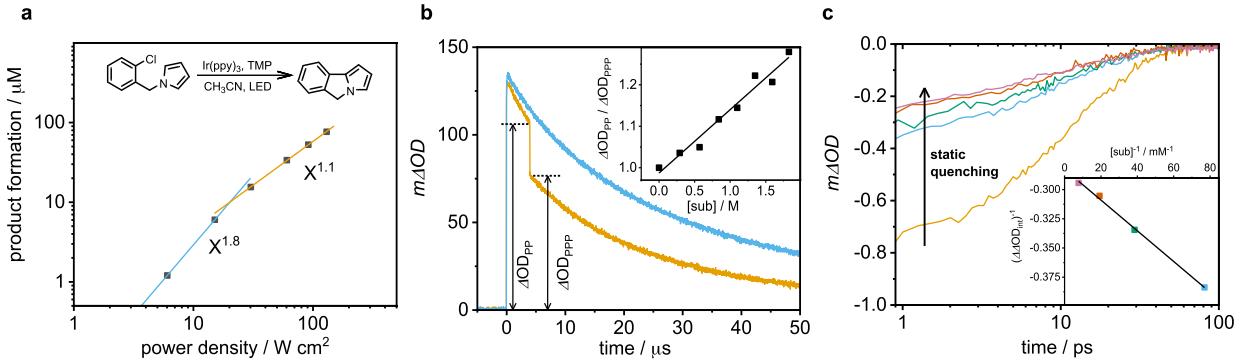

Figure 8. a. Double logarithmic plot of the product concentration of the BHAS reaction of 1-(2-chlorobenzyl)-1H-pyrrole to 5H-pyrrolo[2,1-*a*]isoindole after 30 minutes as a function of excitation power density. **b.** Two-color pump−pump−probe experiment performed at variable electron acceptor concentrations. The arrow illustrates the key observables ΔOD_{pp} (pp = pump−probe, signal intensity just before the second pump pulse) and ΔOD_{ppp} (ppp = pump−pump−probe, signal intensity immediately after the second pump pulse). The inset shows the Stern−Volmer-like plot based on the two-color pump−pump−probe experiment performed at variable electron acceptor concentrations. **c.** Static quenching of the kinetic traces of the transient UV−vis absorption ground state bleach of $DCB^{\bullet-}$ at 760 nm in the presence of different 5H-pyrrolo[2,1-*a*]isoindole substrate concentrations. The inset shows a Benesi−Hildebrand plot assuming a 1:1 preassociation between $DCB^{\bullet-}$ and 5H-pyrrolo[2,1-*a*]isoindole, based on the integrated differences of changes in optical densities ($\Delta\Delta OD_{Int}$). All raw data are summarized from ref.[38]

between 455 and 510 nm may be attributed to the presence of the 10-cyanoanthrolate anion, as they closely match the reference spectrum. Consequently, the absorption features of $[DCA(H)]^-$ within that wavelength range remain unknown, making a direct comparison to the observed reactivity with chlorobenzene challenging. Nonetheless, an electrophotocatalytic study demonstrated that DCA could be utilized as an e-PRC catalyst to activate substrates with excited state potentials down to −2.9 V versus SCE.[27] This is compatible with the formation of $[DCA(H)]^-$. These observations demonstrate the possibility of different reaction mechanisms becoming dominant depending on the substrates, light excitation wavelength, catalytic conditions, and excitation strategy, even though the same photoactive precursor compound was initially present.

https://doi.org/10.1021/jacsau.4c00974
JACS Au 2025, 5, 426−447

In a recent study, we identified 4,4″-dicyano-*p*-terphenyl (DCT) and 4,4′-dicyanobiphenyl (DCB) as strong reductants in their excited radical anionic form.[38] Since both DCT and DCB absorb only in the ultraviolet range, a conventional ConPET strategy is not applicable. Instead, we employed a ConPET approach with a second chromophore to enable the formation of the photoredox active $DCT^{\bullet-}$ and $DCB^{\bullet-}$ under visible light (Figure 1b). These species were then applied in challenging redox-neutral base-promoted homolytic aromatic substitution (BHAS) reactions (Figure 2m). The use of visible light excitation and the absence of classical amine-based electron donors minimize the risk of forming possible photoactive decomposition products.[29,33] Further, mechanistic insights were obtained through a two-photonic process analysis of the BHAS reaction (Figure 8a, inset).[102] The product formation yield versus the excitation power density showed two regimes (Figure 8a): a biphotonic process with a slope of 1.8 and a pseudo monophotonic process with a slope of 1.1 at higher excitation power densities (above 20 W/cm^2). This suggests a high steady state concentration of $DCB^{\bullet-}$ at high laser power, leading to a pseudo monophotonic reaction regime. Such a two-regime observation is often observed for two-photonic mechanisms with relatively long-lived intermediates.[118,119] Spectroscopic evidence for the photoredox activity of the radical ions was provided by two-color pump−pump−probe laser flash photolysis (Figure 8b), similar to an approach used in a previous study.[5] In this experiment, a 355 nm nanosecond laser pulse generated $DCT^{\bullet-}$, which, upon a 4 μs delay, was selectively excited by a 532 nm pulse to form ^{2}*$DCT^{\bullet-}$. This pulse caused significant bleaching of the $DCT^{\bullet-}$ signal in the presence of an electron acceptor (in this case CH_2Cl_2), indicating SET of ^{2}*$DCT^{\bullet-}$. The preassociation of the radical anion with the substrate (in this case 1-(2-chlorobenzyl)-1H-pyrrole) was quantified using femtosecond two-color pump−pump−probe experiments. Here, the kinetic trace of the ground state bleach was detected at 760 nm in the presence of increasing substrate concentrations (Figure 8c). Although decay kinetics remained unchanged up to 130 mM substrate concentration, the amplitude of the transient absorption signal decreased with higher substrate concentrations, suggesting static excited-state quenching. Benesi−Hildebrand analysis assuming a 1:1 preassociation between $DCB^{\bullet-}$ and 5H-pyrrolo[2,1-*a*]isoindole provided an association constant of 185 ± 40 M^{-1} for the radical anion-substrate interaction (Figure 8c, inset). Calculating the free energy of this association using $\Delta G = -RT\ln(K_a)$ (with R as the universal gas constant and T = 293 K), yielded a value of 13 kJ/mol.[120] This value is lower than typical anion-π interaction energies of 20−50 kJ/mol[121] and a reported 21 kJ/mol for aminium radical cation-chlorobenzene interactions.[25] Nevertheless, this indicates a substantial driving force for radical ion−substrate preassociation, which could form the basis for fast static SET in more cases than previously recognized.

Donor−Acceptor Cyanoarene Radical Ions. Donor−acceptor cyanoarene radical ions are a widely applied class of photocatalysts, with numerous examples in the literature.[14,19,20,52−55,57,58,73,74] However, mechanistic studies remain scarce, which is particularly problematic given that cyanoarenes are known to form photoactive decomposition products.[79,122,123] In a recent study, $3CzIPN^{\bullet-}$ and $4DPAIPN^{\bullet-}$ (Figure 2a) were investigated using ultrafast TA spectroscopy.[72] They observed a biexponential decay of the excited radical anion, with a 300 fs component attributed to internal conversion from the higher-lying D_n ($n > 1$) states and an approximately 20 ps component corresponding to the D_1 excited state. However, when examining the transient absorption decay kinetic in the often inaccessible NIR range from 800 to 1600 nm, they found a broad TA signal at 1440 nm, decaying on a much longer time scale (nanosecond range). This observed absorption band at 1440 nm is characteristic of solvated electrons in acetonitrile.[124,125] The quantum yield of solvated electron production was estimated to be 10% for $4CzIPN^{\bullet-}$ and 20% for $4DPAIPN^{\bullet-}$.[72] The excited state lifetime of D_1 and D_n remained unchanged in the presence of an electron acceptor, such as 4-bromoanisole or 4-chloroanisole, with a reduction potential of down to −2.9 V versus SCE.[2] However, the lifetime of the formed solvated electron decreased significantly, from which a reaction rate constant of ∼3.4 × 10^{10} M^{-1} s^{-1} was determined. This indicates a diffusion-based reactivity of the solvated electron,[44,47,126] kinetically outcompeting the excited organic radical anion (Figure 9). Further, TDDFT calculations suggest

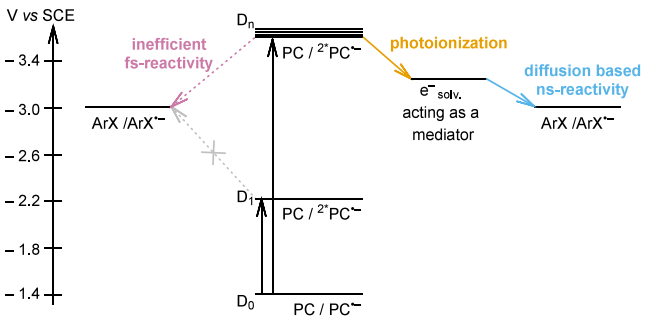

Figure 9. Schematic reactivity of donor−acceptor cyanoarene radical anions based on their redox potentials. The excitation energy of 0.8 eV to the D_1 state corresponds to the lowest-energy transitions of the cyanoarene radical anion, as determined by DFT calculations. The excitation energy of 2.4 eV to the D_n states ($n > 1$) corresponds to the observed visible absorption band of $4CzIPN^{\bullet-}$. The 300 fs excited state lifetime of the D_n state prevents efficient photoinduced electron transfer (purple leftward arrow) to the substrate (ArX). The photoionization (orange rightward arrow) generates a solvated electron storing the extreme redox potential on a nanosecond time scale, acting as a mediator. Now, diffusion-based single electron transfer to the substrate (ArX) can occur (blue arrow).

that photoionization occurs by exciting the system to a higher excited state (D_n), as the lowest excited state with an energy of 0.8 eV shows insufficient redox power to generate the solvated electron (Figure 9).[72] The generation of solvated electrons could be generally feasible for many other reductive organic radicals upon photoexcitation, particularly when extreme excited-state reduction potentials are reached.

4.2. Radical Cations

***N*-Phenylphenothiazine Radical Cation.** *N*-Phenylphenothiazine radical cation ($PTH^{\bullet+}$) is widely used in oxidative photocatalysis as discussed above (Figure 3a). For its D_1-excited state, an oxidation potential of +2.2 V versus SCE is expected (Table 2, entry 5). Next to C−H heteroamination of electron-deficient arenes,[6] or pentafluorosulfanylation reactions,[7,42,86] $PTH^{\bullet+}$ can also be utilized in chloride oxidation reactions (Figure 10).[5] In this study, the authors employed a nanosecond two-color pump−pump−probe experiment, similar as shown in Figure 8b, to explore the SET of ^{2}*$PTH^{\bullet+}$ with Cl^-.[5] Similarly to Figure 8b (inset), with increased chloride concentration a stronger signal bleach was observed. Analogous data analysis revealed a Stern−Volmer constant of 0.36 M^{-1}. Hence, the

https://doi.org/10.1021/jacsau.4c00974
JACS Au 2025, 5, 426−447

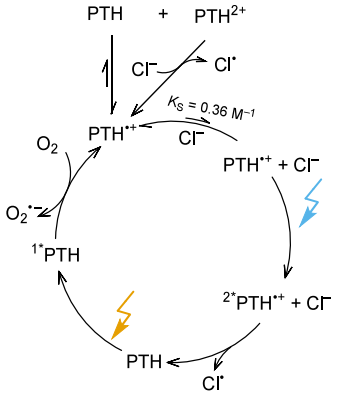

Figure 10. Proposed mechanism of the investigated chloride oxidation using PTH and a ConPET excitation strategy.[5]

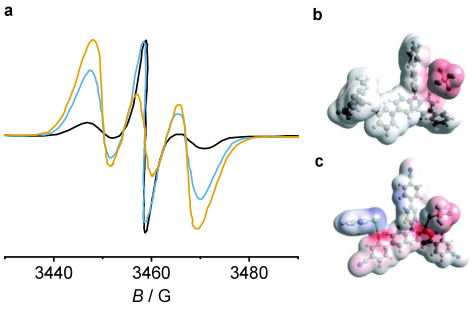

Figure 11. a. EPR spectra of TCBPA$^{\bullet+}$ in the absence (black line) and presence of chlorobenzene (orange line) or 1,2-dichlorobenzene (blue line). The raw data were extracted[106] from ref.[25] **b/c.** DFT spin density plot of TpBPA$^{\bullet+}$ with mesitylene (b) or TCBPA$^{\bullet+}$ with chlorobenzene (c).[25] Copyright 2021 Authors, licensed under a Creative Commons Attribution (CC-BY-3.0) license.

authors concluded preassociation of the PTH$^{\bullet+}$ and chloride ion with an ion-pairing equilibrium constant of K_s = 0.36 M^{-1}.[5]

However, the authors also noted that the persistence time of PTH$^{\bullet+}$ (in its electronic ground state) decreased in the presence of high chloride concentrations. Given that the direct oxidation of chloride by PTH$^{\bullet+}$ is thermodynamically unfavorable by >500 mV, the authors proposed an alternative disproportionation mechanism (Figure 10). In this mechanism, two PTH$^{\bullet+}$ molecules combine to form one neutral PTH and one highly oxidative doubly oxidized PTH^{2+} species. Analysis of PTH's first and second oxidation potentials revealed that the disproportionation equilibrium heavily favors PTH$^{\bullet+}$. Nonetheless, the irreversible chloride oxidation may shift the equilibrium toward PTH^{2+} over the course of a proceeding photoreaction. Using the transient absorption kinetics, the authors estimated the disproportionation equilibrium using a kinetic model. The resulting low disproportionation equilibrium in the presence of chloride of ~5.5 × 10^{-8} M^{-1} is in line with the observed low reaction yields under these conditions.[5] Such disproportionation reactions can, in principle, also occur for other radical ions. However, in most cases, the disproportionation equilibrium of photoactive radical ions is unfavorable. Consequently, such a disproportionation mechanism is unlikely to be the main reaction pathway in most cases of synthetically oriented studies.

Triarylammonium Radical Cations. In recent studies,[36,92] triphenylammonium radical cations (TPA$^{\bullet+}$) were used for the blue light driven activation of substrates that require oxidation potentials > +3.0 V versus SCE (Figure 3a).[36] The observed excited state lifetime of TPA$^{\bullet+}$ around 10 ps rules out diffusion controlled bimolecular reactivity at commonly used substrate concentrations. Hence, the required preassociation between TPA$^{\bullet+}$ and substrate molecules was investigated.

The UV−vis absorption spectrum of TPA$^{\bullet+}$ was recorded in the presence and absence of a substrate. When utilizing TCBPA$^{\bullet+}$ (Figure 3a), a slight shift of the UV−vis absorption signal from 384 to 395 nm was reported upon adding chlorobenzene, suggesting preassociation.[25,36] The EPR signal of TCBPA$^{\bullet+}$ revealed two radical species corresponding to one triplet and one superimposed singlet signal (Figure 11a, black trace). This finding was taken as evidence for the existence of two rotamers. A significant change in the signal shape occurred upon adding chlorobenzene, resulting in the almost exclusive appearance of the triplet signal, which suggests an association of chlorobenzene with one of the two TCBPA$^{\bullet+}$ rotamers (Figure 11a, orange trace).[25,36] Similar, but smaller effects were observed when using 1,2-dichlorobenzene (Figure 11a, blue trace), and only minor differences could be observed using 1,4-dichlorobenzene (not shown). This is in line with the observed decrease in C−H heteroamination reaction yields of 65% (chlorobenzene), 17% (1,2-dichlorobenzene), and 6% (1,4-dichlorobenzene), indicating that substrate preassociation is crucial for the reaction performance. Density functional theory (DFT) calculations were performed with variable substrates to quantify the free energy of the proposed preassociation. A value of approximately 19.2 kJ/mol was obtained for TCBPA$^{\bullet+}$ with chlorobenzene. Additionally, a change in spin density was calculated for TpBPA$^{\bullet+}$ upon substrate aggregation (Figure 11c), which explains the observed changes in the EPR signal and the UV−vis absorption spectrum. Interestingly, this could only be observed with TpBPA$^{\bullet+}$, whereas structurally similar TPA$^{\bullet+}$ shows only minor changes in the EPR signal and no differences in the UV−vis absorption spectra despite the demonstrated reactivity.[25] Nonetheless, preassociation with TPA$^{\bullet+}$ could be shown by DFT calculations. However, no changes in the spin density were found (Figure 11b). Even though the authors showed evidence for the expected preassociation, direct $D_0 \rightarrow D_1$ excitation of different TPA$^{\bullet+}$ photocatalysts resulted in no reactivity. Furthermore, some substrates had oxidation potentials above >3.0 V versus SCE, whereas D_1-excited TdCBA$^{\bullet+}$ can only provide an oxidation power of up to 2.7 V versus SCE (Table 2, entry 7). Hence, the authors speculated that anti-Kasha reactivity might occur from a higher excited state (D_n, $n > 1$) absorbing at 395 nm.[36]

However, another investigation that examined structurally related prephotocatalysts, specifically TPAC(Me)$_2$ (Figure 3a), questioned this interpretation.[92] In this study, ultrafast transient absorption spectroscopy demonstrated reductive quenching of ^{2}*[TPAC(Me)$_2$]$^{\bullet+}$ by 1,2-dimethoxybenzene. This SET was evidenced by the formation of oxidized 1,2-dimethoxybenzene, characterized by an absorption band at 505 nm. This formation of 1,2-dimethoxybenzene radical cation indicates reactivity of ^{2}*[TPAC(Me)$_2$]$^{\bullet+}$, but no changes were observed when using different excitation wavelengths, resulting in the formation of D_1 (700 nm) or D_n (400 nm) excited states, indicating that anti-Kasha reactivity is not occurring in this case.

5. POSSIBLE ANTI-KASHA BEHAVIOR INVOLVING ULTRA-SHORT-LIVED EXCITED STATES

All electronically excited species decay by cumulative relaxations back to their ground state. Any photochemical reaction step leading to a substrate activation must compete with these

https://doi.org/10.1021/jacsau.4c00974
JACS Au 2025, 5, 426−447

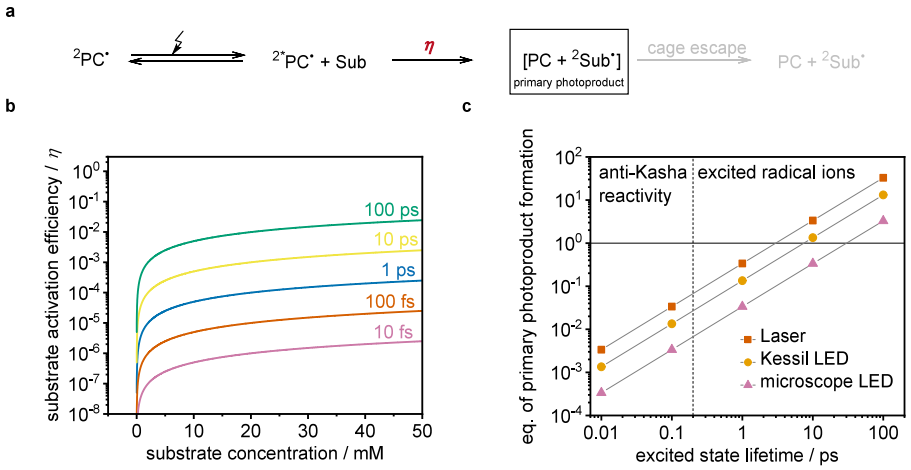

Figure 12. a. Simplified reaction scheme for diffusion-controlled bimolecular SET with radical ion photoactive compounds (PC). For simplicity, the radicals are depicted as ^{2}PC$^\bullet$, representing both the radical anion (^{2}PC$^{\bullet-}$) and the radical cation (^{2}PC$^{\bullet+}$). Initially, the radical ion undergoes photoexcitation, forming the excited radical ion (^{2*}PC$^\bullet$). Diffusion brings the substrate into spatial proximity, to form a so-called "encounter complex", in which SET occurs from the excited radical ion to a substrate (Sub) forming the radical cation or radical anion of the substrate (^{2}Sub$^\bullet$). If the determination of k_q is based on excited-state quenching experiments, the substrate activation efficiency η describes the efficiency for forming the primary photoproducts [PC + ^{2}Sub$^\bullet$], which are still embedded in a solvent cage. The subsequent elementary reaction step of cage escape then liberates the photoproducts. Since the cage escape efficiency is generally not unity,[130] the product formation efficiency is lower than the substrate activation efficiency, though this fact is often ignored.[131] **b.** Diffusion controlled substrate activation efficiency (η) for typical excited state lifetimes and substrate concentrations using eq 1. A diffusion-controlled SET rate constant of 5×10^9 M^{-1} s^{-1} was assumed, a typical value for many organic solvents at room temperature.[129] **c.** Theoretically available equivalents of primary photoproducts per substrate molecule after the initial SET at different excited lifetimes of the radical ions and various light sources with different irradiances (see text for details).

relaxation processes. The ratio η between the substrate activation rate and the total excited-state decay rates can be used as a descriptor of the probability of the excited state to initiate a chemical reaction. For bimolecular reactions, this substrate activation efficiency η can be determined by using eq 1,[118,127,128]

$$\eta = \frac{k_q \times [Q]}{\frac{1}{\tau_0} + k_q \times [Q]} = \frac{\tau_0 - \tau}{\tau_0} \quad (1)$$

where k_q is the bimolecular reaction rate constant in units of M^{-1} s^{-1}, τ_0 is the natural excited state lifetime (i.e., the lifetime in the absence of substrate), and $[Q]$ is the substrate concentration.

To analyze whether diffusion-based SET can occur from excited radical ions, we examine the reaction efficiency (η) at typical excited state lifetimes of radical ions between 1 and 100 ps (Tables 1 and 2). Additionally, excited state lifetimes of 10 and 100 fs were analyzed to assess under what conditions anti-Kasha reactivity from higher excited states might occur.[25,92] As the excited radical ions often show high driving forces for SET reactions (leading to essentially activationless electron transfer), diffusion-controlled reaction rates of $k_q = 5 \times 10^9$ M^{-1} s^{-1} were assumed similar to previous studies.[129] Substrate concentrations between 0 and 50 mM were considered as typical substrate concentrations, in line with most synthetically oriented photoredox studies. The resulting substrate activation efficiencies η for different excited state lifetimes τ_0 are shown in Figure 12b.

For excited state lifetimes of <100 ps, a quenching efficiency of less than 2% is expected at a substrate concentration of 50 mM. Hence, less than every 50th absorbed photon leads to the formation of the primary photoproducts. This substrate activation efficiency η drops even further with the more common radical ion excited state lifetimes of ∼10 ps (Tables 1 and 2) and lower substrate concentrations. This raises the question of whether the initial substrate activation step (Figure 12a) is efficient enough to drive reactions involving such picosecond-lived excited states, even under conditions, where all subsequent elementary steps proceed with 100% efficiency. To address this question, we calculated the maximally expectable number of equivalents of primary photoproduct (Figure 12c) after the initial SET reaction for various light sources with different irradiances and for various excited state lifetimes using eq 2,

$$\text{equiv of primary photoproduct} = \frac{n_{photon} \times \eta}{n_{substrate} \times \nu} \quad (2)$$

where n_{photon} corresponds to the total amount of absorbed photons, η is the substrate activation efficiency, $n_{substrate}$ is the molar quantity of substrate starting material, and ν the number of photons needed per catalytic turnover (in the case of the biphotonic ConPET mechanism $\nu = 2$).

To estimate the total number of photons and substrate molecules involved in a hypothetical reaction, we considered a model reaction setup where a 1 cm^2 area of a total volume of 1 mL is irradiated. These assumptions resemble reactions conducted in optical cuvettes, with a path length of 1 cm, which is a common setup for mechanistic investigations in photoredox catalysis.[127] Assuming a substrate concentration of 50 mM, complete photon absorption, and an irradiation time of 10 h at an excitation wavelength of 447 nm, the amount of absorbed photons (in mol) can be calculated with eq 3,

$$n_{photon} = \frac{P_{light} \times t}{E_{photon} \times N_A} \quad (3)$$

where P_{light} is the power output of different light sources in W, t is the irradiation time (36000 s = 10 h), E_{photon} is the energy of a single photon with a wavelength of 447 nm (4.44×10^{-19} J), and N_A is Avogadro's constant.

https://doi.org/10.1021/jacsau.4c00974
JACS Au 2025, 5, 426−447

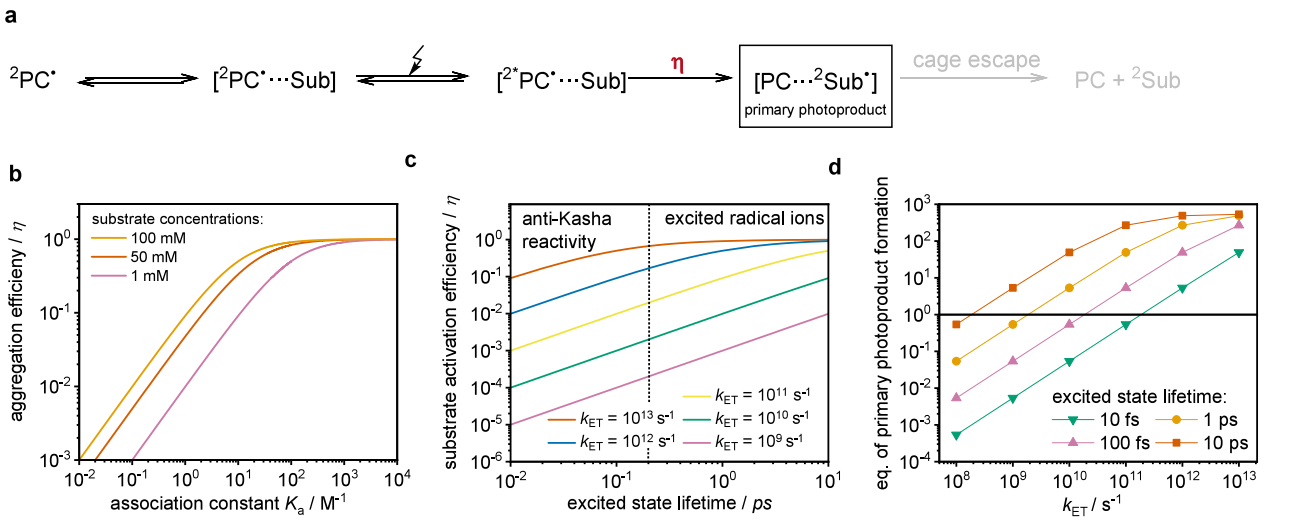

Figure 13. a. Simplified reaction scheme for static SET between radical photocatalysts (^{2}PC$^\bullet$) and substrate molecules (Sub). For simplicity, the radicals are designated as ^{2}PC$^\bullet$, representing both the radical anion (^{2}PC$^{\bullet-}$) and the radical cation ^{2}PC$^{\bullet+}$). First, preassociation needs to occur between ^{2}PC$^\bullet$ and Sub, forming the preaggregate ([^{2}PC$^\bullet$···Sub]). Second, the [^{2}PC$^\bullet$···Sub] gets excited, forming the excited radical ion-substrate aggregate ([^{2*}PC$^\bullet$···Sub]). Subsequently, static SET forms the radical cation or radical anion of the substrate (^{2}Sub$^\bullet$). The substrate activation efficiency η describes the efficiency for forming the primary photoproducts [PC + ^{2}Sub$^\bullet$], which are still embedded in a solvent cage. The subsequent elementary reaction step of cage escape then liberates the photoproducts. Since the cage escape efficiency is generally not unity,[130,131] the product formation efficiency is lower than the substrate activation efficiency, though this fact is often ignored. The primary photoproduct ([PC + ^{2}Sub$^\bullet$]), and the activated substrate can further react upon cage escape. **b.** Preassociation efficiency ($\eta_{preassociaton}$) of ^{2}PC$^\bullet$ and Sub as a function of association constant (K_a) and substrate concentrations. **c.** Static excited state quenching efficiency (η) for different natural excited state lifetimes and substrate concentrations using eq 5. **d.** Theoretically available equivalents of primary photoproducts per substrate molecule after the initial SET at different k_{ET} values and different excited state lifetimes (see text for details).

The total amount of substrate molecules initially present in the reaction mixture can be calculated with eq 4,

$$n_{substrate} = c \times V \tag{4}$$

where c is the substrate concentration (50 mM), and V is the reaction volume (1 mL). Substituting eqs 3 and 4 into eq 2, we then calculated the expectable number of formed equivalents of primary photoproduct as a function of different excited state lifetimes at typical irradiances of commonly used light sources: 2 W cm^{-2} (continuous wave (cw) laser),[132] 400 mW cm^{-2} Kessil lamp, and 100 mW cm^{-2} microscope LED's (Figure 12c).[127]

Equivalence of primary photoproduct greater than 1 indicates an excess of activated substrate with respect to initially present substrate (implying repeated activation of a given substrate molecule during the continuous photoexcitation). In contrast, a value below 1 indicates insufficient primary photoproduct formation to obtain full substrate conversion. At excited state lifetimes below 3 ps, it appears evident that diffusion-based reactivity is not sufficient to drive the catalysis, regardless of the excitation sources used. This is even true when a faster reaction rate of 10^{10} M^{-1} s^{-1} is assumed. However, with excited state lifetimes approaching 100 ps, diffusion-based reactivity might become a possible mechanism. In this scenario, up to 32 times more primary photoproducts can be theoretically formed than the initial number of substrate molecules when using a cw laser and up to 13 times more with a Kessil LED. As a result, even with a typically observed cage escape quantum yield of ~10% (Figure 12a), full conversion can be possible, assuming there are no other major loss channels after cage escape.[130,131,133−135]

A similar analysis can be applied to a scenario where preassociation between the photoactive radical ion and a substrate molecule facilitates static and, consequently, much faster SET to the substrate (Figure 13a). The substrate activation efficiency η, in this case, can be estimated using eq 5:

$$\eta = \frac{k_{ET}}{\tau_0^{-1} + k_{ET}} \times \eta_{preassociation} \tag{5}$$

where τ_0 is the natural excited state lifetime, k_{ET} is the electron transfer rates, and $\eta_{preassociation}$ is the preassociation efficiency between the substrate and the ^{2}PC$^\bullet$.

To estimate the efficiency of preassociation ($\eta_{preassociation}$), the ratio of substrate-^{2}PC$^\bullet$ aggregate concentration ([Sub···^{2}PC$^\bullet$]) to initial ^{2}PC$^\bullet$ concentration ([^{2}PC$^\bullet$]$_{start}$) was calculated using eq 6,

$$\eta_{preaccociation} = \frac{[Sub\cdots{}^2PC^\bullet]}{[{}^2PC^\bullet]_{start}} = \frac{K_a \times [Sub]_{start}}{1 + K_a \times [Sub]_{start}} \tag{6}$$

where K_a is the association constant and [Sub]$_{start}$ is the starting concentration of substrate. The derivation of eq 6 is provided in the (SI).

Using classical concentrations of substrate (1 mM to 100 mM) and ^{2}PC$^\bullet$ (100 μM), the aggregation efficiency was calculated for various association constants (Figure 13b). A value of 1 indicates that each ^{2}PC$^\bullet$ is aggregated with a substrate. With the previously reported association constant of 180 M^{-1} for radical anion-π interactions,[38] a classical substrate concentration of 50 mM and a ^{2}PC$^\bullet$ concentration of 100 μM, approximately 90% of the ^{2}PC$^\bullet$ is preassociated with the substrate. This suggests that preassociation is not necessarily the limiting factor for subpicosecond reactivity, at least at the beginning of the reaction.

Now, the substrate activation efficiency (η) can be calculated using eq 5 as a function of excited state lifetime (τ_0 = 10 fs to 10 ps) for various electron transfer rates (k_{ET} = 10^9 s^{-1} to 10^{13} s^{-1}), assuming a preassociation efficiency of 1 (Figure 13b). For the relatively slow electron transfer rate of 10^{10} s^{-1} and with excited lifetimes above 1 ps, a substrate activation efficiency of above

https://doi.org/10.1021/jacsau.4c00974
JACS Au 2025, 5, 426−447

~1% is observed (Figure 13c, green line). However, when k_{ET} reaches 10^{12} s^{-1},[136] which can occur when the driving force matches the system's reorganization energy (λ) of approximately 0.7 eV,[137,138] efficiencies greater than 1% can, in principle, be expected even with ultrashort excited state lifetimes of 10 to 100 fs (Figure 13b, orange and blue traces). Such short decay times are typical for internal conversion from a higher excited state to lower excited states. The significantly higher driving force for SET from the higher excited states could make anti-Kasha reactivity competitive with their inherent excited state decay, according to our analysis.

With the substrate activation efficiency determined, the theoretically available equivalents of primary photoproducts were calculated for a 400 mW cm^{-2} Kessil LED using eq 2. These values were then plotted against k_{ET} values ranging from 10^8 s^{-1} to 10^{13} s^{-1} for various excited state lifetimes between 10 fs and 10 ps (Figure 13d). For excited radical ions with lifetimes greater than 1 ps, approximately six equivalents of primary photoproducts can be expected when using a Kessil lamp (400 mW cm^{-2}) and assuming a relatively low k_{ET} value of 10^{10} s^{-1}. This relatively high value of 6 underscores the benefit of preassociation between the substrate and the photocatalyst when the excited state decays rapidly (i.e., < 10 ps). Interestingly, even higher excited states with ultrashort lifetimes of 10 to 100 fs can still form the primary photoproduct effectively, producing approximately 5 to 60 equiv of the theoretical primary photoproduct when a k_{ET} value of 10^{12} s^{-1} is assumed. As a result, even with a typical 10% cage escape quantum yield, anti-Kasha reactivity seems plausible using a simple Kessil LED, assuming there are no other major loss channels after cage escape,[130,131,133−135] potentially opening a door to new photochemistry that was previously unthinkable. The key requirement seems to be quite simply efficient preaggregation between the photoactive species and the substrate.

6. CONCLUSION AND OUTLOOK

Excited radicals have long been recognized as potentially important photoactive species that might become useful for photocatalysis.[32,34,40,85,87,89] However, it was not until 2014, with the introduction of a synthetically oriented ConPET excitation strategy, that excited radicals were rediscovered as potent compounds in organic photoredox catalysis.[22] Synthetic studies reveal a broad application potential for excited radical ions using the ConPET or the e-PRC strategy. Nevertheless, in-depth mechanistic studies on excited radicals have identified different possible reaction pathways.[24,25,30,35,38,43] These include forming decomposition products which can act as photocatalysts,[29,76,90,113−115] disproportionation reactions leading to doubly oxidized or reduced species,[5] or the formation of solvated electrons.[17,72]

Our analysis suggests that the primary mechanism may vary throughout the reaction or depending on the substrate used. This variability presents challenges for mechanistic studies, as time-dependent spectroscopy techniques such as nanosecond two-color pump−pump−probe experiments,[5,38] or femtosecond transient absorption experiments[35,38,67,92] usually only reveal the possible reaction pathway at the start of a photocatalysis. However, this pathway can significantly change over the irradiation time. As a result, these experiments may not necessarily elucidate the primary reaction mechanism throughout the entire irradiation period relevant to synthetic conditions. This may be achieved by monitoring product formation as a function of irradiation time while observing the generation of the primary photoactive species, in this case, the radical ions.[30,66,139] In scenarios where product formation follows the decay of the photocatalyst concentration, it indicates that a decomposition product drives the reaction.[30] Conversely, when increased reactivity correlates with higher levels of formed radical ions, it provides evidence that the radical is responsible for the photoreactivity. Another approach is observing product formation at different excitation wavelengths (indicated in Figure 7c/d). The absorption spectrum of the photoactive species should reflect the observed reaction yield when the same power densities are used.[24,140] However, such an analysis may be inconclusive for the biphotonic ConPET excitation strategy, as the first photon absorption event is often much more efficient than the second. When using two photosensitizers, they might show different absorption behavior. Hence, this methodology may be more applicable when photoredox active radical ions are generated chemically or electrochemically.[24] For the ConPET excitation strategy, a quadratic power dependency may serve as a relatively straightforward means to investigate the biphotonic nature of the ConPET mechanism,[67,102] keeping in mind that deviations from this behavior can occur at high excitation densities.[38] Problematically, such quadratic dependencies are expected for many different types of biphotonic mechanisms, including biphotonic mechanisms that originate from the formation of photodegradation products.[122,123] Hence, combining time-resolved spectroscopy with the arguably simpler observation of product yields at different irradiation times, excitation wavelengths, or power densities can provide a more comprehensive picture of the dominant mechanism over a typical irradiation time of multiple hours. Obtaining a more complete understanding of the dominant mechanisms may lead to designing more efficient catalytic systems and discovering novel and more efficient photocatalysts or mechanistic pathways.

Arguably, the extremely short excited state lifetimes of organic radicals remain a significant challenge in the rational design of novel catalytic systems. Our analysis indicates that excited state lifetimes of less than 10 ps necessitate preassociation of the organic radical photocatalyst with the substrate, as diffusion-based SET is too slow for efficient catalysis. Understanding and developing effective preassociation strategies remains a significant limitation in developing efficient catalytic systems utilizing organic radicals. Effective preassociation of organic radical photocatalysts with substrates could enable faster SET even on the ultrafast time scale of 10−100 fs, as demonstrated by our analysis (Figure 13). Rapid SET within photocatalyst-substrate aggregates might indeed facilitate reactivity from higher excited states (D_n, $n > 1$), a phenomenon known as anti-Kasha reactivity.[141] Anti-Kasha reactivity leads to significantly higher redox potentials because it allows more energy to be retained in the catalytic system, enhancing energy efficiency by preventing nonradiative decay to the lowest excited state (Figure 14). This effect has been recognized in zinc(II) porphyrins, where anti-Kasha emission from the S_2 state, with a relatively slow internal conversion with an excited state lifetime of 1.5 ps.[142] In this case, subpicosecond SET can be observed in covalently linked and preassociation-based donor/acceptor systems.[143−153] Additionally, such anti-Kasha reactivity has been applied for SET initiation reactions in polymerization.[153] For such a fast reaction to occur, an SET rate constant of 10^{12} s^{-1} is necessary. Achieving such fast rate constants requires an SET driving force on the order of the typical reorganization energy of

https://doi.org/10.1021/jacsau.4c00974
JACS Au 2025, 5, 426−447

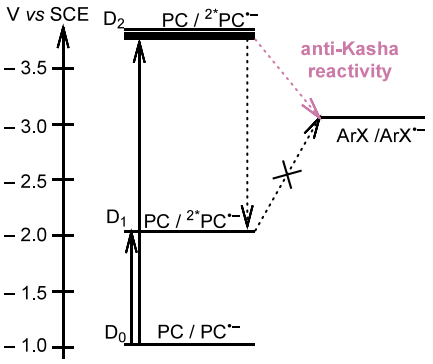

Figure 14. Concept of anti-Kasha reactivity for excited radical anions. Upon generating the photoactive radical anion, the lowest excited state (D_1) is populated using low-energy photons, with the excited state redox potential dependent on the stored light energy. Exciting the radical anion to its D_2 state with high energy photons allows for storing additional photon energy, potentially leading to extreme reduction potentials. Such reactivity could exceed the redox power of the D_1 excited state of the same photocatalyst. However, the SET (purple dotted arrow) needs to compete against the inherent decay back to the lowest excited state D_1 (black dotted arrow).

approximately 0.7 eV to achieve a barrierless SET.[138] In classical excited radical anions, the energy difference between D_1 and D_2 excited states can be as large as 1.5 eV, making this a realistic scenario. Further, the excited state lifetime of higher excited states may be increased by introducing symmetry that forbids the transition of the higher excited state, increasing the likelihood of anti-Kasha reactivity.[154−156]

Applying this principle to organic radicals could unlock extreme redox potentials, enabling selective reactivity for applications such as chiral resolution, selective decomposition of persistent pollutants, or addressing particularly challenging SET reactions, provided that efficient preassociation can be precisely controlled.

■ ASSOCIATED CONTENT

Supporting Information

The Supporting Information is available free of charge at https://pubs.acs.org/doi/10.1021/jacsau.4c00974.

The derivation of eq 6 (PDF)

■ AUTHOR INFORMATION

Corresponding Authors

Björn Pfund − *Department of Chemistry, University of Basel, 4056 Basel, Switzerland;* Present Address: Department of Chemistry, Michigan State University, East Lansing, Michigan 48824, United States; orcid.org/0000-0003-0936-2975; Email: pfundbjo@msu.edu

Oliver S. Wenger − *Department of Chemistry, University of Basel, 4056 Basel, Switzerland;* orcid.org/0000-0002-0739-0553; Email: oliver.wenger@unibas.ch

Complete contact information is available at: https://pubs.acs.org/10.1021/jacsau.4c00974

Author Contributions

CRediT: **Björn Pfund** conceptualization, data curation, formal analysis, funding acquisition, investigation, visualization, writing - original draft, writing - review & editing; **Oliver S. Wenger** conceptualization, formal analysis, funding acquisition, project administration, resources, writing - review & editing.

Notes

The authors declare no competing financial interest.

■ ACKNOWLEDGMENTS

B.P. thanks the National Research Fund Luxembourg for a Ph. D. grant (14583224) and the Swiss National Science Foundation (P500PN_225730) for a postdoc mobility fellowship. O.S.W. acknowledges funding by the Swiss National Science Foundation (grant number 200020_207329 and 10001855).

■ REFERENCES

(1) Shen, T.; Lambert, T. H. Electrophotocatalytic diamination of vicinal C−H bonds. *Science* **2021**, *371*, 620−626.

(2) MacKenzie, I. A.; Wang, L.; Onuska, N. P. R.; Williams, O. F.; Begam, K.; Moran, A. M.; Dunietz, B. D.; Nicewicz, D. A. Discovery and characterization of an acridine radical photoreductant. *Nature* **2020**, *580*, 76−80.

(3) Huang, H.; Lambert, T. H. Electrophotocatalytic S_NAr Reactions of Unactivated Aryl Fluorides at Ambient Temperature and Without Base. *Angew. Chem., Int. Ed.* **2020**, *59*, 658−662.

(4) Huang, H.; Strater, Z. M.; Rauch, M.; Shee, J.; Sisto, T. J.; Nuckolls, C.; Lambert, T. H. Electrophotocatalysis with a Trisaminocyclopropenium Radical Dication. *Angew. Chem., Int. Ed.* **2019**, *58*, 13318−13322.

(5) Li, P.; Deetz, A. M.; Hu, J.; Meyer, G. J.; Hu, K. Chloride Oxidation by One- or Two-Photon Excitation of *N*-Phenylphenothiazine. *J. Am. Chem. Soc.* **2022**, *144*, 17604−17610.

(6) Targos, K.; Williams, O. P.; Wickens, Z. K. Unveiling Potent Photooxidation Behavior of Catalytic Photoreductants. *J. Am. Chem. Soc.* **2021**, *143*, 4125−4132.

(7) Rombach, D.; Wagenknecht, H.-A. Photoredox Catalytic α-Alkoxypentafluorosulfanylation of α-Pethyl- and α-Phenylstyrene Using SF_6. *Angew. Chem., Int. Ed.* **2020**, *59*, 300−303.

(8) Christensen, J. A.; Phelan, B. T.; Chaudhuri, S.; Acharya, A.; Batista, V. S.; Wasielewski, M. R. Phenothiazine Radical Cation Excited States as Super-oxidants for Energy-Demanding Reactions. *J. Am. Chem. Soc.* **2018**, *140*, 5290−5299.

(9) Baek, Y.; Reinhold, A.; Tian, L.; Jeffrey, P. D.; Scholes, G. D.; Knowles, R. R. Singly Reduced Iridium Chromophores: Synthesis, Characterization, and Photochemistry. *J. Am. Chem. Soc.* **2023**, *145*, 12499−12508.

(10) Neumeier, M.; Sampedro, D.; Májek, M.; de la Peña O'Shea, V. A.; Jacobi von Wangelin, A.; Pérez-Ruiz, R. Dichromatic Photocatalytic Substitutions of Aryl Halides with a Small Organic Dye. *Chem.—Eur. J.* **2018**, *24*, 105−108.

(11) Ilic, A.; Schwarz, J.; Johnson, C.; de Groot, L. H. M.; Kaufhold, S.; Lomoth, R.; Wärnmark, K. Photoredox catalysis via consecutive ^{2}LMCT- and ^{3}MLCT-excitation of an Fe(III/II)-N-heterocyclic carbene complex. *Chem. Sci.* **2022**, *13*, 9165−9175.

(12) Venditto, N. J.; Liang, Y. S.; El Mokadem, R. K.; Nicewicz, D. A. Ketone-Olefin Coupling of Aliphatic and Aromatic Carbonyls Catalyzed by Excited-State Acridine Radicals. *J. Am. Chem. Soc.* **2022**, *144*, 11888−11896.

(13) Cole, J. P.; Chen, D.-F.; Kudisch, M.; Pearson, R. M.; Lim, C.-H.; Miyake, G. M. Organocatalyzed Birch Reduction Driven by Visible Light. *J. Am. Chem. Soc.* **2020**, *142*, 13573−13581.

(14) Soika, J.; McLaughlin, C.; Neveselý, T.; Daniliuc, C. G.; Molloy, J. J.; Gilmour, R. Organophotocatalytic N−O Bond Cleavage of Weinreb Amides: Mechanism-Guided Evolution of a PET to ConPET Platform. *ACS Catal.* **2022**, *12*, 10047−10056.

(15) Ghosh, I.; König, B. Chromoselective Photocatalysis: Controlled Bond Activation through Light-Color Regulation of Redox Potentials. *Angew. Chem., Int. Ed.* **2016**, *55*, 7676−7679.

(16) Bardagi, J. I.; Ghosh, I.; Schmalzbauer, M.; Ghosh, T.; König, B. Anthraquinones as Photoredox Catalysts for the Reductive Activation of Aryl Halides. *Eur. J. Org. Chem.* **2018**, *2018*, 34−40.
(17) Naumann, R.; Kerzig, C.; Goez, M. Laboratory-scale photoredox catalysis using hydrated electrons sustainably generated with a single green laser. *Chem. Sci.* **2017**, *8*, 7510−7520.
(18) Giedyk, M.; Narobe, R.; Weiß, S.; Touraud, D.; Kunz, W.; König, B. Photocatalytic activation of alkyl chlorides by assembly-promoted single electron transfer in microheterogeneous solutions. *Nat. Catal.* **2020**, *3*, 40−47.
(19) Xu, J.; Cao, J.; Wu, X.; Wang, H.; Yang, X.; Tang, X.; Toh, R. W.; Zhou, R.; Yeow, E. K. L.; Wu, J. Unveiling Extreme Photoreduction Potentials of Donor-Acceptor Cyanoarenes to Access Aryl Radicals from Aryl Chlorides. *J. Am. Chem. Soc.* **2021**, *143*, 13266−13273.
(20) Chmiel, A. F.; Williams, O. P.; Chernowsky, C. P.; Yeung, C. S.; Wickens, Z. K. Non-innocent Radical Ion Intermediates in Photoredox Catalysis: Parallel Reduction Modes Enable Coupling of Diverse Aryl Chlorides. *J. Am. Chem. Soc.* **2021**, *143*, 10882−10889.
(21) Tian, X.; Karl, T. A.; Reiter, S.; Yakubov, S.; de Vivie-Riedle, R.; König, B.; Barham, J. P. Electro-mediated PhotoRedox Catalysis for Selective C(sp^3)-O Cleavages of Phosphinated Alcohols to Carbanions. *Angew. Chem., Int. Ed.* **2021**, *60*, 20817−20825.
(22) Ghosh, I.; Ghosh, T.; Bardagi, J. I.; König, B. Reduction of aryl halides by consecutive visible light-induced electron transfer processes. *Science* **2014**, *346*, 725−728.
(23) Li, H.; Wenger, O. S. Photophysics of Perylene Diimide Dianions and Their Application in Photoredox Catalysis. *Angew. Chem., Int. Ed.* **2022**, *61*, No. e202110491.
(24) Horsewill, S. J.; Hierlmeier, G.; Farasat, Z.; Barham, J. P.; Scott, D. J. Shining Fresh Light on Complex Photoredox Mechanisms through Isolation of Intermediate Radical Anions. *ACS Catal.* **2023**, *13*, 9392−9403.
(25) Wu, S.; Žurauskas, J.; Domański, M.; Hitzfeld, P. S.; Butera, V.; Scott, D. J.; Rehbein, J.; Kumar, A.; Thyrhaug, E.; Hauer, J.; et al. Hole-mediated photoredox catalysis: tris(*p*-substituted)biarylaminium radical cations as tunable, precomplexing and potent photooxidants. *Org. Chem. Front.* **2021**, *8*, 1132−1142.
(26) Costentin, C.; Fortage, J.; Collomb, M. N. Electrophotocatalysis: Cyclic Voltammetry as an Analytical Tool. *J. Phys. Chem. Lett.* **2020**, *11*, 6097−6104.
(27) Kim, H.; Kim, H.; Lambert, T. H.; Lin, S. Reductive Electrophotocatalysis: Merging Electricity and Light To Achieve Extreme Reduction Potentials. *J. Am. Chem. Soc.* **2020**, *142*, 2087−2092.
(28) Cowper, N. G. W.; Chernowsky, C. P.; Williams, O. P.; Wickens, Z. K. Potent Reductants via Electron-Primed Photoredox Catalysis: Unlocking Aryl Chlorides for Radical Coupling. *J. Am. Chem. Soc.* **2020**, *142*, 2093−2099.
(29) Rieth, A. J.; Gonzalez, M. I.; Kudisch, B.; Nava, M.; Nocera, D. G. How Radical Are "Radical" Photocatalysts? A Closed-Shell Meisenheimer Complex Is Identified as a Super-Reducing Photoreagent. *J. Am. Chem. Soc.* **2021**, *143*, 14352−14359.
(30) Marchini, M.; Gualandi, A.; Mengozzi, L.; Franchi, P.; Lucarini, M.; Cozzi, P. G.; Balzani, V.; Ceroni, P. Mechanistic insights into two-photon-driven photocatalysis in organic synthesis. *Phys. Chem. Chem. Phys.* **2018**, *20*, 8071−8076.
(31) Freccero, M.; Mella, M.; Albini, A. The Photochemical Reactions of 9,10-Anthracenedicarbonitrile and 1,4-Naphthalenedicarbonitrile in Acetonitrile in the Presence of Bases. *Tetrahedron* **1994**, *50*, 2115−2130.
(32) Fujitsuka, M.; Majima, T. Reaction dynamics of excited radical ions revealed by femtosecond laser flash photolysis. *J. Photochem. Photobiol. C* **2018**, *35*, 25−37.
(33) Beckwith, J. S.; Aster, A.; Vauthey, E. The excited-state dynamics of the radical anions of cyanoanthracenes. *Phys. Chem. Chem. Phys.* **2021**, *24*, 568−577.
(34) Fujitsuka, M.; Kim, S. S.; Lu, C.; Tojo, S.; Majima, T. Intermolecular and Intramolecular Electron Transfer Processes from Excited Naphthalene Diimide Radical Anions. *J. Phys. Chem. B* **2015**, *119*, 7275−7282.
(35) Zeman, C. J.; Kim, S.; Zhang, F.; Schanze, K. S. Direct Observation of the Reduction of Aryl Halides by a Photoexcited Perylene Diimide Radical Anion. *J. Am. Chem. Soc.* **2020**, *142*, 2204−2207.
(36) Wu, S.; Kaur, J.; Karl, T. A.; Tian, X.; Barham, J. P. Synthetic Molecular Photoelectrochemistry: New Frontiers in Synthetic Applications, Mechanistic Insights and Scalability. *Angew. Chem., Int. Ed.* **2022**, *61*, No. e202107811.
(37) Lepori, M.; Schmid, S.; Barham, J. P. Photoredox catalysis harvesting multiple photon or electrochemical energies. *Beilstein J. Org. Chem.* **2023**, *19*, 1055−1145.
(38) Pfund, B.; Gejsnaes-Schaad, D.; Lazarevski, B.; Wenger, O. S. Monitoring picosecond reactions of excited radical ion super reductants in photocatalysis. *Nat. Commun.* **2024**, *15*, 4738.
(39) Huang, H.; Steiniger, K. A.; Lambert, T. H. Electrophotocatalysis: Combining Light and Electricity to Catalyze Reactions. *J. Am. Chem. Soc.* **2022**, *144*, 12567−12583.
(40) Berger, R. M.; McMillin, D. R.; Dallinger, R. F. Two-Photon Photochemistry of $[Cu(dmp)_2]^+$. *Inorg. Chem.* **1987**, *26*, 3802−3805.
(41) Pellegrin, Y.; Odobel, F. Sacrificial electron donor reagents for solar fuel production. *C. R. Chimie* **2017**, *20*, 283−295.
(42) Rombach, D.; Wagenknecht, H. A. Photoredox Catalytic Activation of Sulfur Hexafluoride for Pentafluorosulfanylation of α-Methyl- and α-Phenyl Styrene. *ChemCatChem.* **2018**, *10*, 2955−2961.
(43) Glaser, F.; Wenger, O. S. Red Light-Based Dual Photoredox Strategy Resembling the Z-Scheme of Natural Photosynthesis. *JACS Au* **2022**, *2*, 1488−1503.
(44) Kerzig, C.; Goez, M. Combining energy and electron transfer in a supramolecular environment for the "green" generation and utilization of hydrated electrons through photoredox catalysis. *Chem. Sci.* **2016**, *7*, 3862−3868.
(45) Favereau, L.; Makhal, A.; Pellegrin, Y.; Blart, E.; Petersson, J.; Göransson, E.; Hammarström, L.; Odobel, F. A. Molecular Tetrad That Generates a High-Energy Charge-Separated State by Mimicking the Photosynthetic Z-Scheme. *J. Am. Chem. Soc.* **2016**, *138*, 3752−3760.
(46) Zeng, L.; Huang, L.; Huang, Z.; Mani, T.; Huang, K.; Duan, C.; Han, G. Long wavelength near-infrared and red light-driven consecutive photo-induced electron transfer for highly effective photoredox catalysis. *Nat. Commun.* **2024**, *15*, 7270.
(47) Goez, M.; Kerzig, C.; Naumann, R. An "all-green" catalytic cycle of aqueous photoionization. *Angew. Chem., Int. Ed.* **2014**, *53*, 9914−9916.
(48) Barham, J. P.; König, B. Synthetic Photoelectrochemistry. *Angew. Chem., Int. Ed.* **2020**, *59*, 11732−11747.
(49) Rehm, D.; Weller, A. Kinetics of fluorescence quenching by electron and H-atom transfer. *Isr. J. Chem.* **1970**, *8*, 259−271.
(50) Elgrishi, N.; Rountree, K. J.; McCarthy, B. D.; Rountree, E. S.; Eisenhart, T. T.; Dempsey, J. L. A Practical Beginner's Guide to Cyclic Voltammetry. *J. Chem. Educ.* **2018**, *95*, 197−206.
(51) Gosztola, D.; Niemczyk, M. P.; Svec, W.; Lukas, A. S.; Wasielewski, M. R. Excited Doublet States of Electrochemically Generated Aromatic Imide and Diimide Radical Anions. *J. Phys. Chem. A* **2000**, *104*, 6545−6551.
(52) Qu, Z.; Tian, T.; Tan, Y.; Ji, X.; Deng, G.-J.; Huang, H. Redox-neutral ketyl radical coupling/cyclization of carbonyls with *N*-aryl acrylamides through consecutive photoinduced electron transfer. *Green Chem.* **2022**, *24*, 7403−7409.
(53) Ma, C.; Tian, Y.; Wang, J.; He, X.; Jiang, Y.; Yu, B. Visible-Light-Driven Transition-Metal-Free Site-Selective Access to Isonicotinamides. *Org. Lett.* **2022**, *24*, 8265−8270.
(54) Mayerhofer, V. J.; Lippolis, M.; Teskey, C. J. Dual-Catalysed Intermolecular Reductive Coupling of Dienes and Ketones. *Angew. Chem., Int. Ed.* **2024**, *63*, No. e202314870.
(55) Fang, Y.; Liu, T.; Chen, L.; Chao, D. Exploiting consecutive photoinduced electron transfer (ConPET) in CO_2 photoreduction. *Chem. Commun.* **2022**, *58*, 7972−7975.

https://doi.org/10.1021/jacsau.4c00974
JACS Au 2025, 5, 426−447

(56) Chatterjee, A.; König, B. Birch-Type Photoreduction of Arenes and Heteroarenes by Sensitized Electron Transfer. *Angew. Chem., Int. Ed.* **2019**, *58*, 14289−14294.
(57) Chernowsky, C. P.; Chmiel, A. F.; Wickens, Z. K. Electrochemical Activation of Diverse Conventional Photoredox Catalysts Induces Potent Photoreductant Activity. *Angew. Chem., Int. Ed.* **2021**, *60*, 21418−21425.
(58) Chen, L.; Qu, Q.; Ran, C. K.; Wang, W.; Zhang, W.; He, Y.; Liao, L. L.; Ye, J. H.; Yu, D. G. Photocatalytic Carboxylation of C-N Bonds in Cyclic Amines with CO_2 by Consecutive Visible-Light-Induced Electron Transfer. *Angew. Chem., Int. Ed.* **2023**, *62*, No. e202217918.
(59) Gong, H.-X.; Cao, Z.; Li, M.-H.; Liao, S.-H.; Lin, M.-J. Photoexcited perylene diimide radical anions for the reduction of aryl halides: a bay-substituent effect. *Org. Chem. Front.* **2018**, *5*, 2296−2302.
(60) Zeng, L.; Liu, T.; He, C.; Shi, D.; Zhang, F.; Duan, C. Organized Aggregation Makes Insoluble Perylene Diimide Efficient for the Reduction of Aryl Halides via Consecutive Visible Light-Induced Electron-Transfer Processes. *J. Am. Chem. Soc.* **2016**, *138*, 3958−3961.
(61) Liu, Z.; Li, X.; Yin, W.; Chen, J.; Li, C.; Cheng, F.; Liu, J. J. Perylenediimide-Based Hybrid Materials for the Iodoperfluoroalkylation of Alkenes and Oxidative Coupling of Amines: Bay-Substituent-Mediated Photocatalytic Activity. *ACS Appl. Mater. Interfaces* **2022**, *14*, 53090−53100.
(62) Rosso, C.; Filippini, G.; Cozzi, P. G.; Gualandi, A.; Prato, M. Highly Performing Iodoperfluoroalkylation of Alkenes Trigger Triggered by the Photochemical Activity of Perylene Diimides. *ChemPhotoChem.* **2019**, *3*, 193−197.
(63) Li, Z.-J.; Li, S.; Hofman, E.; Hunter Davis, A.; Leem, G.; Zheng, W. Visible-light induced disproportionation of pyrrole derivatives for photocatalyst-free aryl halides reduction. *Green Chem.* **2020**, *22*, 1911−1918.
(64) Pathania, V.; Roy, V. J.; Roy, S. R. Transforming Non-innocent Phenalenyl to a Potent Photoreductant: Captivating Reductive Functionalization of Aryl Halides through Visible-Light-Induced Electron Transfer Processes. *J. Org. Chem.* **2022**, *87*, 16550−16566.
(65) Caby, S.; Marin Oliva, L.; Bardagi, J. I. Unravelling the Effect of Water Addition in Consecutive Photocatalysis with Naphthalene Diimide. *J. Org. Chem.* **2023**, *88*, 711−716.
(66) Caby, S.; Bouchet, L. M.; Argüello, J. E.; Rossi, R. A.; Bardagi, J. I. Excitation of Radical Anions of Naphthalene Diimides in Consecutive- and Electro-Photocatalysis. *ChemCatChem.* **2021**, *13*, 3001−3009.
(67) Jeong, D. Y.; Lee, D. S.; Lee, H. L.; Nah, S.; Lee, J. Y.; Cho, E. J.; You, Y. Evidence and Governing Factors of the Radical-Ion Photoredox Catalysis. *ACS Catal.* **2022**, *12*, 6047−6059.
(68) Shaikh, R. S.; Düsel, S. J. S.; König, B. Visible-Light Photo-Arbuzov Reaction of Aryl Bromides and Trialkyl Phosphites Yielding Aryl Phosphonates. *ACS Catal.* **2016**, *6*, 8410−8414.
(69) Das, A.; Ghosh, I.; König, B. Synthesis of pyrrolo[1,2-*a*]quinolines and ullazines by visible light mediated one- and twofold annulation of *N*-arylpyrroles with arylalkynes. *Chem. Commun.* **2016**, *52*, 8695−8698.
(70) Graml, A.; Ghosh, I.; König, B. Synthesis of Arylated Nucleobases by Visible Light Photoredox Catalysis. *J. Org. Chem.* **2017**, *82*, 3552−3560.
(71) Herrera-Luna, J. C.; Díaz, D. D.; Jiménez, M. C.; Pérez-Ruiz, R. Highly Efficient Production of Heteroarene Phosphonates by Dichromatic Photoredox Catalysis. *ACS Appl. Mater. Interfaces* **2021**, *13*, 48784−48794.
(72) Villa, M.; Fermi, A.; Calogero, F.; Wu, X.; Gualandi, A.; Cozzi, P. G.; Troisi, A.; Ventura, B.; Ceroni, P. Organic super-reducing photocatalysts generate solvated electrons via two consecutive photon induced processes. *Chem. Sci.* **2024**, *15*, 14739−14745.
(73) Huang, C.; Xiao, P.; Ye, Z. M.; Wang, C. L.; Kang, C.; Tang, S.; Wei, Z.; Cai, H. Direct C(sp^3)-H Arylation of Unprotected Benzyl Anilines and Alkylarenes by Organocatalysis under Visible Light. *Org. Lett.* **2024**, *26*, 304−309.
(74) Xian, N.; Yin, J.; Ji, X.; Deng, G. J.; Huang, H. Visible-Light-Mediated Photoredox Carbon Radical Formation from Aqueous Sulfoxonium Ylides. *Org. Lett.* **2023**, *25*, 1161−1165.
(75) Brandl, F.; Bergwinkl, S.; Allacher, C.; Dick, B. Consecutive Photoinduced Electron Transfer (conPET): The Mechanism of the Photocatalyst Rhodamine 6G. *Chem.—Eur. J.* **2020**, *26*, 7946−7954.
(76) Sau, A.; Pompetti, N. F.; Green, A. R.; Popescu, M. V.; Paton, R. S.; Miyake, G. M.; Damrauer, N. H. Mechanistic Investigation of a Photocatalyst Model Reveals Function by Perylene-Like Closed Shell Super-Photoreductant Capable of Reducing Unactivated Arenes. *ACS Catal.* **2024**, *14*, 2252−2263.
(77) Moneo, A.; Carvalho, M. F. N. N.; Telo, J. P. Dicyanoaromatic radical anions as mixed valence species. *J. Phys. Org. Chem.* **2012**, *25*, 559−565.
(78) Wang, Y.; Zhao, Z.; Pan, D.; Wang, S.; Jia, K.; Ma, D.; Yang, G.; Xue, X. S.; Qiu, Y. Metal-Free Electrochemical Carboxylation of Organic Halides in the Presence of Catalytic Amounts of an Organomediator. *Angew. Chem., Int. Ed.* **2022**, *61*, No. e202210201.
(79) Kwon, Y.; Lee, J.; Noh, Y.; Kim, D.; Lee, Y.; Yu, C.; Roldao, J. C.; Feng, S.; Gierschner, J.; Wannemacher, R.; et al. Formation and degradation of strongly reducing cyanoarene-based radical anions towards efficient radical anion-mediated photoredox catalysis. *Nat. Commun.* **2023**, *14*, 92.
(80) Sheng, H.; Liu, Q.; Zhang, B. B.; Wang, Z. X.; Chen, X. Y. Visible-Light-Induced N-Heterocyclic Carbene-Catalyzed Single Electron Reduction of Mono-Fluoroarenes. *Angew. Chem., Int. Ed.* **2023**, *62*, No. e202218468.
(81) Huang, H.; Lambert, T. H. Electrophotocatalytic Acetoxyhydroxylation of Aryl Olefins. *J. Am. Chem. Soc.* **2021**, *143*, 7247−7252.
(82) Huang, H.; Strater, Z. M.; Lambert, T. H. Electrophotocatalytic C-H Functionalization of Ethers with High Regioselectivity. *J. Am. Chem. Soc.* **2020**, *142*, 1698−1703.
(83) Huang, H.; Lambert, T. H. Regiodivergent Electrophotocatalytic Aminooxygenation of Aryl Olefins. *J. Am. Chem. Soc.* **2022**, *144*, 18803−18809.
(84) Shen, T.; Li, Y. L.; Ye, K. Y.; Lambert, T. H. Electrophotocatalytic oxygenation of multiple adjacent C-H bonds. *Nature* **2023**, *614*, 275−280.
(85) Moutet, J.-C.; Reverdy, G. Photochemistry of cation radicals in solution: photoinduced oxidation by the phenothiazine cation radical. *Tetrahedron Lett.* **1979**, *20*, 2389−2392.
(86) Rombach, D.; Birenheide, B.; Wagenknecht, H. A. Photoredox Catalytic Pentafluorosulfanylative Domino Cyclization of α-Substituted Alkenes to Oxaheterocycles by Using SF_6. *Chem.—Eur. J.* **2021**, *27*, 8088−8093.
(87) Moutet, J.-C.; Reverdy, G. Photochemistry of Cation Radicals in Solution: Photoinduced Electron-transfer Reactions between Alcohols and the *N,N,N′,N′*-Tetraphenyl-*p*-phenylenediamine Cation Radical. *J. Chem. Soc. Chem. Commun.* **1982**, *0*, 654−655.
(88) Salehzadeh, H.; Mashhadizadeh, M. H. Nitrone Synthesis via Pair Electrochemical Coupling of Nitro-Compounds with Benzyl Alcohol Derivatives. *J. Org. Chem.* **2019**, *84*, 9307−9312.
(89) Fox, M. A. The Photoexcited States of Organic Anions. *Chem. Rev.* **1979**, *79*, 253−273.
(90) Breslin, D. T.; Fox, M. A. Excited-State Behavior of Thermally Stable Radical Ions. *J. Phys. Chem.* **1994**, *98*, 408−411.
(91) Shukla, S. S.; Rusling, J. F. Photoelectrocatalytlc Reduction of 4-Chlorobiphenyl Using Anion Radicals and Visible Light. *J. Phys. Chem.* **1985**, *89*, 3353−3358.
(92) Bieszczad, B.; Karl, T. A.; Rolka, A. B.; Nuernberger, P.; Kutta, R. J.; König, B. Oxidative con-PET Catalysis for Arene Functionalization. *ChemRxiv* **2022**, DOI: 10.26434/chemrxiv-2022-39x5l.
(93) Shine, H. J.; Zhao, D.-C. Electron Transfer to Excited Doublet States. Photoirradiation of 10-Methylphenothiazine Cation Radical Perchlorate in Solutions of Phenylacetylene and *p*-Tolylacetylene in Acetonitrile. *J. Org. Chem.* **1990**, *55*, 4086−4089.
(94) Ogawa, T.; Sinha, N.; Pfund, B.; Prescimone, A.; Wenger, O. S. Molecular Design Principles to Elongate the Metal-to-Ligand Charge Transfer Excited-State Lifetimes of Square-Planar Nickel(II) Complexes. *J. Am. Chem. Soc.* **2022**, *144*, 21948−21960.
(95) Schepp, N. P.; Johnston, L. J. Reactivity of Radical Cations. Effect of Radical Cation and Alkene Structure on the Absolute Rate Constants

https://doi.org/10.1021/jacsau.4c00974
JACS Au 2025, 5, 426−447

of Radical Cation Mediated Cycloaddition Reactions. *J. Am. Chem. Soc.* **1996**, *118*, 2872−2881.
(96) Fukuzumi, S.; Yuasa, J.; Satoh, N.; Suenobu, T. Scandium Ion-Promoted Photoinduced Electron Transfer from Electron Donors to Acridine and Pyrene. Essential Role of Scandium Ion in Photocatalytic Oxygenation of Hexamethylbenzene. *J. Am. Chem. Soc.* **2004**, *126*, 7585−7594.
(97) Chung, Y. C.; Su, Y. O. Effects of Phenyl- and Methyl-Substituents on *p*-Phenylenediamine, an Electrochemical and Spectral Study. *J. Chin. Chem. Soc.* **2009**, *56*, 493−503.
(98) Liu, T.; Xue, F.; Wang, B.; Wang, R.; Cao, W.; Zhao, X.; Xia, Y.; Jin, W.; Zhang, Y.; Lin, H.; et al. Rapid microwave synthesis of Bi_2WO_6 for C = C bonds oxidative cleavage to ketones with visible light irradiation in aerobic micellar medium. *J. Catal.* **2023**, *417*, 41−51.
(99) Kasha, M. Characterization of electronic transitions in complex molecules. *Discuss. Faraday Soc.* **1950**, *9*, 14−19.
(100) Kandoth, N.; Pérez Hernández, J.; Palomares, E.; Lloret-Fillol, J. Mechanisms of photoredox catalysts: the role of optical spectroscopy. *J. Sustain. Energy* **2021**, *5*, 638−665.
(101) Beil, S. B.; Bonnet, S.; Casadevall, C.; Detz, R. J.; Eisenreich, F.; Glover, S. D.; Kerzig, C.; Næsborg, L.; Pullen, S.; Storch, G.; et al. Challenges and Future Perspectives in Photocatalysis: Conclusions from an Interdisciplinary Workshop. *JACS Au* **2024**, *4*, 2746.
(102) Glaser, F.; Kerzig, C.; Wenger, O. S. Multi-Photon Excitation in Photoredox Catalysis: Concepts, Applications, Methods. *Angew. Chem., Int. Ed.* **2020**, *59*, 10266−10284.
(103) Talbott, E. D.; Burnett, N. L.; Swierk, J. R. Mechanistic and kinetic studies of visible light photoredox reactions. *Chem. Phys. Rev.* **2023**, *4*, 031312.
(104) Balzani, V.; Bolletta, F.; Scandola, F. Vertical and "Nonvertical" Energy Transfer Processes. A General Classical Treatment. *J. Am. Chem. Soc.* **1980**, *102*, 2152−2163.
(105) Rosspeintner, A.; Angulo, G.; Vauthey, E. Bimolecular photoinduced electron transfer beyond the diffusion limit: the Rehm-Weller experiment revisited with femtosecond time resolution. *J. Am. Chem. Soc.* **2014**, *136*, 2026−2032.
(106) Data were extracted from the corresponding figure. https://automeris.io/WebPlotDigitizer/index.html, 2024.
(107) Connell, T. U.; Fraser, C. L.; Czyz, M. L.; Smith, Z. M.; Hayne, D. J.; Doeven, E. H.; Agugiaro, J.; Wilson, D. J. D.; Adcock, J. L.; Scully, A. D.; et al. The Tandem Photoredox Catalysis Mechanism of $[Ir(ppy)_2(dtb\text{-}bpy)]^+$ Enabling Access to Energy Demanding Organic Substrates. *J. Am. Chem. Soc.* **2019**, *141*, 17646−17658.
(108) Glaser, F.; Larsen, C. B.; Kerzig, C.; Wenger, O. S. Aryl dechlorination and defluorination with an organic super-photoreductant. *Photochem. Photobiol. Sci.* **2020**, *19*, 1035−1041.
(109) Cozzi, P. G.; Calogero, F.; Wilczek, L.; Pinosa, E.; Gualandi, A.; Dorta, R.; Herrera, A.; Dai, Y.; Rossignol, A.; Negri, F.; et al. Stable Meisenheimer Complexes as Powerful Photoreductants Readily Obtained from Aza-Heteroaromatic Compounds. *Angew. Chem., Int. Ed.* **2024**, *63*, No. e202411074.
(110) Biswas, A.; Kolb, S.; Röttger, S. H.; Das, A.; Patalag, L. K.; Dey, P. P.; Sil, S.; Maji, S.; Chakraborty, S.; Wenger, O. S.; Bhunia, A.; Werz, D. B.; Mandal, S. K. A BOIMPY Dye Enables Multi-Photoinduced Electron Transfer Catalysis: Reaching Super-Reducing Properties. *Angew. Chem. Int. Ed.* **2025**, e202416472.
(111) Eriksen, J.; Lund, H.; Nyvad, A. I.; Yamato, T.; Mitchell, R. H.; Dingle, T. W.; Williams, R. V.; Mahedevan, R. Electron-Transfer Fluorescence Quenching of Radical Ions. *Acta Chem. Scand. B* **1983**, *37b*, 459−466.
(112) Eriksen, J.; Joergensen, K. A.; Linderberg, J.; Lund, H. Electron-Transfer Fluorescence Quenching of Radical Ions. Experimental Work and Theoretical Calculations. *J. Am. Chem. Soc.* **1984**, *106*, 5083−5087.
(113) Fujita, M.; Ishida, A.; Majima, T.; Takamuku, S. Lifetimes of Radical Anions of Dicyanoanthracene, Phenazine, and Anthraquinone in the Excited State from the Selective Electron-Transfer Quenching. *J. Phys. Chem.* **1996**, *100*, 5382−5387.
(114) Schmalzbauer, M.; Svejstrup, T. D.; Fricke, F.; Brandt, P.; Johansson, M. J.; Bergonzini, G.; König, B. Redox-Neutral Photocatalytic C−H Carboxylation of Arenes and Styrenes with CO_2. *Chem.* **2020**, *6*, 2658−2672.
(115) Schmalzbauer, M.; Ghosh, I.; König, B. Utilising excited state organic anions for photoredox catalysis: activation of (hetero)aryl chlorides by visible light-absorbing 9-anthrolate anions. *Faraday Discuss.* **2019**, *215*, 364−378.
(116) Breslin, B. T.; Fox, M. A. A Strongly Chemiluminescent Dioxetanimine Dianion Fragmentation: Reaction of the Dicyanoanthracene Radical Anion with Superoxide Ion. *J. Am. Chem. Soc.* **1993**, *115*, 11716−11721.
(117) Hodge, S. A.; Buckley, D. J.; Yau, H. C.; Skipper, N. T.; Howard, C. A.; Shaffer, M. S. P. Chemical routes to discharging graphenides. *Nanoscale* **2017**, *9*, 3150−3158.
(118) Pfund, B.; Hutskalova, V.; Sparr, C.; Wenger, O. S. Isoacridone dyes with parallel reactivity from both singlet and triplet excited states for biphotonic catalysis and upconversion. *Chem. Sci.* **2023**, *14*, 11180−11191.
(119) Singh-Rachford, T. N.; Castellano, F. N. Photon upconversion based on sensitized triplet−triplet annihilation. *Coord. Chem. Rev.* **2010**, *254*, 2560−2573.
(120) Thordarson, P. Determining association constants from titration experiments in supramolecular chemistry. *Chem. Soc. Rev.* **2011**, *40*, 1305−1323.
(121) Schottel, B. L.; Chifotides, H. T.; Dunbar, K. R. Anion-π interactions. *Chem. Soc. Rev.* **2008**, *37*, 68−83.
(122) Grotjahn, S.; König, B. Photosubstitution in Dicyanobenzene-based Photocatalysts. *Org. Lett.* **2021**, *23*, 3146−3150.
(123) Pinosa, E.; Bassan, E.; Cetin, S.; Villa, M.; Potenti, S.; Calogero, F.; Gualandi, A.; Fermi, A.; Ceroni, P.; Cozzi, P. G. Light-Induced Access to Carbazole-1,3-dicarbonitrile: A Thermally Activated Delayed Fluorescent (TADF) Photocatalyst for Cobalt-Mediated Allylations. *J. Org. Chem.* **2023**, *88*, 6390−6400.
(124) Grills, D. C.; Lymar, S. V. Solvated Electron in Acetonitrile: Radiation Yield, Absorption Spectrum, and Equilibrium between Cavity- and Solvent-Localized States. *J. Phys. Chem. B* **2022**, *126*, 262−269.
(125) Doan, S. C.; Schwartz, B. J. Nature of Excess Electrons in Polar Fluids: Anion-Solvated Electron Equilibrium and Polarized Hole-Burning in Liquid Acetonitrile. *J. Phys. Chem. Lett.* **2013**, *4*, 1471−1776.
(126) Kerzig, C.; Guo, X.; Wenger, O. S. Unexpected Hydrated Electron Source for Preparative Visible-Light Driven Photoredox Catalysis. *J. Am. Chem. Soc.* **2019**, *141*, 2122−2127.
(127) Schreier, M. R.; Pfund, B.; Steffen, D. M.; Wenger, O. S. Photocatalytic Regeneration of a Nicotinamide Adenine Nucleotide Mimic with Water-Soluble Iridium(III) Complexes. *Inorg. Chem.* **2023**, *62*, 7636−7643.
(128) Zhang, L.; Pfund, B.; Wenger, O. S.; Hu, X. Oxidase-Type C-H/C-H Coupling Using an Isoquinoline-Derived Organic Photocatalyst. *Angew. Chem., Int. Ed.* **2022**, *61*, No. e202202649.
(129) Montalti, M.; Credi, A.; Prodi, L.; Gandolfi, T. M. *Handbook of Photochemistry*; CRC/Taylor & Francis: Boca Raton, 2006.
(130) Goodwin, M. J.; Dickenson, J. C.; Ripak, A.; Deetz, A. M.; McCarthy, J. S.; Meyer, G. J.; Troian-Gautier, L. Factors that Impact Photochemical Cage Escape Yields. *Chem. Rev.* **2024**, *124*, 7379−7464.
(131) Wang, C.; Li, H.; Bürgin, T. H.; Wenger, O. S. Cage escape governs photoredox reaction rates and quantum yields. *Nat. Chem.* **2024**, *16*, 1151−1159.
(132) Pfund, B.; Steffen, D. M.; Schreier, M. R.; Bertrams, M. S.; Ye, C.; Börjesson, K.; Wenger, O. S.; Kerzig, C. UV Light Generation and Challenging Photoreactions Enabled by Upconversion in Water. *J. Am. Chem. Soc.* **2020**, *142*, 10468−10476.
(133) Olmsted, J., III; Meyer, T. J. Factors Affecting Cage Escape Yields following Electron-Transfer Quenching. *J. Phys. Chem.* **1987**, *91*, 1649−1655.
(134) Lewis, F. D.; Dykstra, R. E.; Gould, I. R.; Farid, S. Cage Escape Yields and Direct Observation of Intermediates in Photoinduced Electron-Transfer Reactions of *cis*- and *trans*-Stilbene. *J. Phys. Chem.* **1988**, *92*, 7042−7043.

(135) Gould, I. R.; Moody, R.; Farid, S. Electron-Transfer Reactions in the Marcus Inverted Region: Differences in Solvation and Electronic Coupling between Excited Charge-Transfer Complexes and Geminate Radical Ion Pairs. *J. Am. Chem. Soc.* **1988**, *110*, 7242−7244.
(136) Gray, H. B.; Winkler, J. R. Long-range electron transfer. *Proc. Natl. Acad. Sci. U.S.A.* **2005**, *102*, 3534−3539.
(137) Gould, I. R.; Moser, J. E.; Armitage, B.; Farid, S.; Goodman, J. L.; Herman, M. S. Electron-transfer reactions in the Marcus inverted region. Charge recombination versus charge shift reactions. *J. Am. Chem. Soc.* **1989**, *111*, 1917−1919.
(138) Marcus, R. A.; Sutin, N. Electron transfers in chemistry and biology. *Biochim. Biophys. Acta* **1985**, *811*, 265−322.
(139) Lei, P.; Hedlund, M.; Lomoth, R.; Rensmo, H.; Johansson, O.; Hammarström, L. The Role of Colloid Formation in the Photoinduced H_2 Production with a Ru^{II}-Pd^{II} Supramolecular Complex: A Study by GC, XPS, and TEM. *J. Am. Chem. Soc.* **2008**, *130*, 26−27.
(140) Protti, S.; Ravelli, D.; Fagnoni, M. Wavelength dependence and wavelength selectivity in photochemical reactions. *Photochem. Photobiol. Sci.* **2019**, *18*, 2094−2101.
(141) Demchenko, A. P.; Tomin, V. I.; Chou, P. T. Breaking the Kasha Rule for More Efficient Photochemistry. *Chem. Rev.* **2017**, *117*, 13353−13381.
(142) Bajema, L.; Gouterman, M.; Rose, C. B Porphyrins XXIII: Fluorescence of the second excited singlet and quasiline structure of zinc tetrabenzporphin. *J. Mol. Spectrosc.* **1971**, *39*, 421−431.
(143) Chosrowjan, H.; Tanigichi, S.; Okada, T.; Takagi, S.; Arai, T.; Tokumam, K. Electron transfer quenching of S_2 state fluorescence of Zn-tetraphenylporphyrin. *Chem. Phys. Lett.* **1995**, *242*, 644−649.
(144) Petersson, J.; Eklund, M.; Davidsson, J.; Hammarström, L. Ultrafast Electron Transfer Dynamics of a Zn(II)porphyrin-Viologen Complex Revisited: S_2 vs S_1 Reactions and Survival of Excess Excitation Energy. *J. Phys. Chem. B* **2010**, *114*, 14329−14338.
(145) Wallin, S.; Monnereau, C.; Blart, E.; Gankou, J. R.; Odobel, F.; Hammarström, L. State-Selective Electron Transfer in an Unsymmetric Acceptor-Zn(II)porphyrin-Acceptor Triad: Toward a Controlled Directionality of Electron Transfer from the Porphyrin S_2 and S_1 States as a Basis for a Molecular Switch. *J. Phys. Chem. A* **2010**, *114*, 1709−1721.
(146) Sugunan, S. K.; Robotham, B.; Sloan, R. P.; Szmytkowski, J.; Ghiggino, K. P.; Paige, M. F.; Steer, R. P. Photophysics of untethered ZnTPP-fullerene complexes in solution. *J. Phys. Chem. A* **2011**, *115*, 12217−12227.
(147) Mataga, N.; Taniguchi, S.; Chosrowjan, H.; Osuka, A.; Yoshida, N. Ultrafast charge transfer and radiationless relaxations from higher excited state (S_2) of directly linked Zn-porphyrin (ZP)-acceptor dyads: investigations into fundamental problems of exciplex chemistry. *Chem. Phys.* **2003**, *295*, 215−228.
(148) Nieto-Pescador, J.; Abraham, B.; Pistner, A. J.; Rosenthal, J.; Gundlach, L. Electronic state dependence of heterogeneous electron transfer: injection from the S_1 and S_2 state of phlorin into TiO_2. *Phys. Chem. Chem. Phys.* **2015**, *17*, 7914−7923.
(149) Rogozina, M. V.; Ionkin, V. N.; Ivanov, A. I. What factors control product yield in charge separation reaction from second excited state in zinc-porphyrin derivatives? *J. Phys. Chem. A* **2012**, *116*, 1159−1167.
(150) Andersson, M.; Davidsson, J.; Korppi-Tommola, J.; Peltola, T.; Hammarström, L. Photoinduced Electron Transfer Reactions in a Porphyrin-Viologen Complex: Observation of S_2 to S_1 Relaxation and Electron Transfer from the S_2 State. *J. Phys. Chem. B* **1999**, *103*, 3258−3262.
(151) Hayes, R. T.; Walsh, C. J.; Wasielewski, M. R. Competitive Electron Transfer from the S_2 and S_1 Excited States of Zinc *meso*-Tetraphenylporphyrin to a Covalently Bound Pyromellitimide: Dependence on Donor-Acceptor Structure and Solvent. *J. Phys. Chem. A* **2004**, *108*, 2375−2381.
(152) Fujitsuka, M.; Cho, D. W.; Tojo, S.; Inoue, A.; Shiragami, T.; Yasuda, M.; Majima, T. Electron Transfer from Axial Ligand to S_1 - and S_2 -Excited Phosphorus Tetraphenylporphyrin. *J. Phys. Chem. A* **2007**, *111*, 10574−10579.
(153) Awwad, N.; Bui, A. T.; Danilov, E. O.; Castellano, F. N. Visible-Light-Initiated Free-Radical Polymerization by Homomolecular Triplet-Triplet Annihilation. *Chem.* **2020**, *6*, 3071−3085.
(154) Dunlop, D.; Ludvikova, L.; Banerjee, A.; Ottosson, H.; Slanina, T. Excited-State (Anti)Aromaticity Explains Why Azulene Disobeys Kasha's Rule. *J. Am. Chem. Soc.* **2023**, *145*, 21569−21575.
(155) Wang, K.; You, X.; Miao, X.; Yi, Y.; Peng, S.; Wu, D.; Chen, X.; Xu, J.; Sfeir, M. Y.; Xia, J. Activated Singlet Fission Dictated by Anti-Kasha Property in a Rylene Imide Dye. *J. Am. Chem. Soc.* **2024**, *146*, 13326−13335.
(156) Zhang, X.; Chen, C.; Zhang, W.; Yin, N.; Yuan, B.; Zhuang, G.; Wang, X. Y.; Du, P. Anomalous anti-Kasha excited-state luminescence from symmetry-breaking heterogeneous carbon bisnanohoops. *Nat. Commun.* **2024**, *15*, 2684.

https://doi.org/10.1021/jacsau.4c00974
JACS Au 2025, 5, 426−447